MICROCOPY RESOLUTION TEST CHART

NATIONAL BUREAU OF STANDARDS-1963-A

ARL-TR-85-6

Copy No. 20

THE EXPERIMENTAL INVESTIGATION OF THE INVERSE PROBLEM IN ROUGH SURFACE SCATTERING OF ACOUSTIC WAVES

Ricky S. Bailey

APPLIED RESEARCH LABORATORIES
THE UNIVERSITY OF TEXAS AT AUSTIN
POST OFFICE BOX 8029, AUSTIN, TEXAS 78713-8029

August 1985

Technical Report

Prepared for:

AD-A158 070

DTIC
ELECTE
AUG 1 5 1985

85   8   12   064

UNCLASSIFIED

REPORT DOCUMENTATION PAGE	READ INSTRUCTIONS BEFORE COMPLETING FORM

1. REPORT NUMBER	2. GOVT ACCESSION NO. $AI58070$	3. RECIPIENT'S CATALOG NUMBER

4. TITLE (and Subtitle)	5. TYPE OF REPORT & PERIOD COVERED
THE EXPERIMENTAL INVESTIGATION OF THE INVERSE PROBLEM OF ROUGH SURFACE SCATTERING OF ACOUSTIC WAVES	technical report
	6. PERFORMING ORG. REPORT NUMBER ARL-TR-85-6

7. AUTHOR(s)	8. CONTRACT OR GRANT NUMBER(s)
Ricky S. Bailey	N00014-80-C-0490

9. PERFORMING ORGANIZATION NAME AND ADDRESS	10. PROGRAM ELEMENT, PROJECT, TASK AREA & WORK UNIT NUMBERS
Applied Research Laboratories The University of Texas at Austin Austin, Texas 78713-8029	Task 18

11. CONTROLLING OFFICE NAME AND ADDRESS	12. REPORT DATE
Office of Naval Research Department of the Navy Arlington, VA 22217	August 1985
	13. NUMBER OF PAGES 91

14. MONITORING AGENCY NAME & ADDRESS(if different from Controlling Office)	15. SECURITY CLASS. (of this report)
	UNCLASSIFIED
	15a. DECLASSIFICATION/DOWNGRADING SCHEDULE

16. DISTRIBUTION STATEMENT (of this Report)

Approved for public release; distribution unlimited.

17. DISTRIBUTION STATEMENT (of the abstract entered in Block 20, if different from Report)

18. SUPPLEMENTARY NOTES

19. KEY WORDS (Continue on reverse side if necessary and identify by block number)

forward scattering	probability density function	Bojarsky-Lewis method
inverse scattering	rms surface height	extended Prony method
rough surface	correlation length	spectral estimation
correlation function	discrete Fourier transform	power spectrum

20. ABSTRACT (Continue on reverse side if necessary and identify by block number)

This study represents an inverse problems approach to rough surface acoustical scattering, the objective being to infer certain statistical characteristics of a randomly rough surface directly from the coherently scattered pressure field. Eckart's physical-acoustical scattering model is applied to derive relationships for the probability density function and correlation function of surface heights which can be inferred directly from the scattered pressure field. Signal processing techniques are used to obtain estimates of the probability density

UNCLASSIFIED

19. (cont'd)

mean scattered pressure
covariance of scattered pressure

20. (cont'd)

function and correlation functions from experimental data. The
experimental measurements are made of the steady-state complex scattered
pressure field from a single frequency small beamwidth source incident upon
a pressure release model rough surface. Comparisons are made between the
characteristics inferred from the scattered pressure and the actual surface
characteristics. The ability of the signal processing techniques to
accurately predict the known characteristics is then evaluated.

TABLE OF CONTENTS

LIST OF FIGURES

v

LIST OF TABLES

vii

ACKNOWLEDGMENT

PREVIOUS PAGE
IS BLANK

I. INTRODUCTION

The direct or forward problem in acoustics is the prediction of the propagation of sound based on specified source, scatterer, and medium conditions. The inverse problem is the deduction of properties of the source, scatterer, and medium from the propagated field. This relationship can be described with the mapping of one function into another, AX=Y, where X represents the specified source, scatterer, and medium properties and Y represents the results of the propagated field. The operator A provides the mapping from X to Y for the direct problem. Inversion of A leads to the solution of the inverse problem.

Although the inverse problem has been the subject of much study,[1-4] most of the work in acoustics has been devoted to the forward problem. Since Lord Rayleigh predicted the scattered field from a sinusoidal surface in 1896,[5] the study of rough surface scattering in particular has resulted in an almost uncountable number of publications and about as many theoretical developments.[6-21] This concentration of study has been no less intense in underwater acoustics where theories have been developed to understand the scattering from the ocean surface and seafloor. A concise review of work accomplished in this area before 1970 was compiled by Fortuin[6] and Horton.[7]

The theories used in these studies have been separated into two basic

categories according to the mathematical approach. The first approach is to model the scattering with a distribution of point scatterers, each with its own impulse response and directivity. Middleton[8] is regarded as the originator of this rather straightforward approach, often called the quasiphenomenalogical approach. The second approach, called the optical-acoustic or physical approach, was formulated by Eckart.[9] In this method the scattered field is described by Helmholtz's theorem and evaluated with Kirchhoff's boundary conditions resulting in integral equations convergent for directional sources.

This latter approach has been widely used by underwater acousticians. At Applied Research Laboratories, The University of Texas at Austin (ARL:UT), a group of investigators have successfully applied Eckart's theory to yield theoretical models which follow experimental data very well.[11-14] These studies, which began in the 1960's, have produced one thesis[15] and two dissertations[16,17] at The University of Texas. Clay and Medwin[18,19] and others[20,21] have also verified Eckart's theory with experimentation.

In these studies of the forward problem the incident acoustic wave and the acoustical and statistical properties of the scattering medium were assumed in an attempt to predict the scattered field. The inverse problem presented in the current work differs in that a limited knowledge of both incident and scattered pressure is assumed in efforts to infer the scatterer's characteristics. In particular, the statistical properties of randomly rough surfaces are the parameters which are of interest.

Experimental studies of the forward problem at ARL:UT were accomplished with model surfaces constructed from aeromagnetic maps of the Canadian Shield,[22] which have been measured for a particular root mean square (rms) surface height and correlation length. These surfaces are also used in the inverse scattering problem, the subject of this thesis. An overview of the acoustical theory supporting the inverse problem is discussed, and solutions are proposed for obtaining estimates of the rms height and correlation length. An experiment was conducted to check the validity of the inverse theory and results from each of the surfaces are compared with each other as well as with the expected results.

place on the data to reduce the leakage.[28]

2. Bojarsky-Lewis Method

Sometimes even with the proper choice of a data window it is still not practical to use the DFT technique to estimate an FT or an inverse FT. For instance, if the data record is so short that leakage cannot be corrected (i.e., through deconvolution), other high resolution spectral estimation techniques must be invoked to estimate the Fourier transform. One method is the Bojarsky-Lewis method (BL),[29] which has been applied in three-dimensional image reconstruction of electromagnetic wave scattering, extrapolation of bandlimited functions, and spectral estimation.

The Bojarsky-Lewis PDF estimate is derived in Appendix A and is represented with the summation

$$\omega(\zeta) = \sum_{j=0}^{J} \langle v(\zeta) , S^{(1)}_{0j}(2\pi\xi_m\zeta_{max}, \zeta/\zeta_{max}) \rangle$$

$$\times (2j+1)S^{(1)}_{0j}(2\pi\xi_m\zeta_{max}, \zeta/\zeta_{max})/2 \quad , \qquad \text{III.6}$$

where the inner product $\langle ... \rangle$ is defined by

$$\langle a , b \rangle = \int_{-\zeta_{max}}^{+\zeta_{max}} a(\zeta) b(\zeta) d\zeta \quad , \qquad \text{III.7}$$

$$\omega(j\zeta) = \Delta\zeta \left[\sum_{\ell=0}^{M-1} \Omega^*(\ell\zeta) \exp[-i2\pi\ell j/M] \right]^* , \quad j = 0, \dots, M-1 \quad , \quad \text{III.5}$$

where $\Omega(\ell\zeta)$ represents the sampled version of Ω consisting of M samples, * denotes complex conjugate, $\Delta\zeta$ denotes the even sampling increment on Ω, and $\Delta\zeta = 1/M\Delta\xi$. The sampled version of ω, $\omega(j\zeta)$, will consist of M samples corresponding to harmonically fixed values of $\zeta = j\Delta\zeta$. Both Ω and ω are by definition periodic functions of period $M\Delta\xi$ and $1/\Delta\xi$ respectively. Proper sampling of Ω will therefore result if the Nyquist criterion of $1/\Delta\xi \geq 2\zeta_{max}$ is followed, where ζ_{max} represents the maximum value of the surface relief (or $\omega(\zeta) = 0$ for $-\zeta_{max} \leq \zeta \leq \zeta_{max}$, a ζ-limited (ζL) function). Otherwise aliasing of ω will occur, and $\omega(j\zeta)$ will not accurately represent ω.

A major problem which is encountered in application of the DFT is the phenomenon of leakage, which occurs due to the finite extent of the data. The leakage results from the multiplication of Ω with a rectangular window function which in the ζ domain corresponds with a convolution of ω with $\sin(2\pi\xi_m\zeta)/\pi\zeta$ (a sinc(ζ) function), where $\xi_m = (\xi_{max} + \xi_{min})/2$. As the observation window ξ_m approaches infinity the sinc function approximates a delta function and leakage contributes very little to the error in the DFT. However, it is not practical at times to extend the data to infinity, and so an optimal window can be chosen to place on the data to

16

estimates of the PDF of heights. In most practical situations Ω is not known for all values of ξ. A study for which the characteristic function is known for various values of frequency (discrete values of ξ) is presented in Reference 19. The objective of the current study is to vary the angles of incidence and reflection only over a modest range of observation to establish measurements of the characteristic function. So the characteristic function is sampled over a ξ-limited (ξL) range, $\xi_{min} \leq \xi \leq \xi_{max}$. The limits are selected so that Ω is bounded, or so that the image solution does not approach zero (due to the finite beamwidth of the directional source).

These limitations of the sampling of the characteristic function indicate that there may likely be a resolution problem in obtaining accurate estimates of the probability density function. The following discussion outlines the discrete Fourier transform and two techniques used in high resolution spectral estimation of the Fourier transform.

1. Discrete Fourier Transform

The Fourier transform theory can then be extended to include sampled functions through the sampling theorem and the discrete Fourier transform (DFT).[27] The definition of the DFT pair follows

$$\Omega(\ell\xi) = \Delta\xi \sum_{j=0}^{M-1} \omega(j\xi) \exp[-i2\pi\ell j/M] \ , \ \ell = 0, \dots , M-1 \qquad \text{III.4}$$

and

image solution, Eq. II.20 becomes

$$\Omega(\xi) = \langle P_S \rangle / P_R \qquad \text{III.1}$$

or

$$\Omega(\xi) = \int_{-\infty}^{+\infty} \omega(\zeta) \exp[-i2\pi\xi\zeta] \, d\zeta \qquad \text{III.2}$$

where the surface wave number $\xi=\gamma/\lambda$ is a function of the angles of incidence and reflection and frequency. If the characteristic function Ω is known for all values of ξ (all angles and all frequencies), ω, the probability density function, is determined by the inverse FT

$$\omega(\zeta) = \int_{-\infty}^{+\infty} \Omega(\xi) \exp[i2\pi\xi\zeta] \, d\xi \qquad . \qquad \text{III.3}$$

A sufficient condition for the validity of Eqs. III.2 and III.3 is found in Papoulis.[26] If the absolute integral of $\omega(\zeta)$ is bounded and finite (absolute integrability), then its FT $\Omega(\xi)$ exists and must satisfy the inverse FT. Since the PDF of surface heights is bounded for a finite surface, its integral will also be bounded, and Eqs. III.2 and III.3 hold.

Thus the inversion of the Fourier transform operator will yield

III. INVERSE TECHNIQUES

Much can be inferred about the scattering surface from the two stochastic quantities derived for the scattered pressure field. In particular, the rms surface height and correlation length can be extracted from measurements of the mean scattered pressure and covariance, respectively. The rms surface height is the square root of the mean squared height of the surface profile and can be obtained from the probability density function of surface heights. The correlation length is a measure of the distance one must move along a rough surface to lose all knowledge of one's previous position and can be directly obtained from the correlation function of surface heights. The signal processing methods used to estimate these parameters are the subject of this chapter.

A. Probability Density Function

The probability density function (PDF) describes the distribution of the surface heights and can be derived from the mean scattered pressure (Section II.B). The PDF is the inverse Fourier transform of the characteristic function; the conjugate Fourier transform variables are surface height ζ, and surface wave number ξ. In the surface wave number domain, the characteristic function is defined as the mean scattered pressure divided by the image solution, P_R, of scattering from a planar surface. So the development is picked up from Eq. II.20 and, for a non-zero

It can be shown that for a suitable random rough surface (i.e., homogeneous, isotropic) the covariance is dependent only upon the difference $|r-r'|$, while for the autocovariance, the peak of the function occurs at a zero-spatial difference ($r=r'$) and corresponds with the scattered pressure intensity. The covariance decreases rapidly as the lag value (spatial difference) increases, the rate of decrease of the function being greater for a larger roughness (ζ_{rms}/λ increasing). Clay and Medwin have shown that for a time varying rough surface, the spatial covariance reaches a maximum at a predictable spatial lag value if the pressures for which the covariance is calculated are fixed time-delay versions of the pressure field. In other words, the pressure is being scattered from the same type of roughness (i.e., a traveling wave or surface structure) at different times into different spatial positions. From calculations of the correlation function of the scattered pressure field, Clay and Medwin were able to predict the wave velocity of a traveling surface wave.

For scattering from a stationary rough surface, the surface correlation is retrieved by spatially correlating the scattered pressure from separately insonified areas on the surface. The value of the correlation function for a particular surface displacement is the peak value of the spatial correlation function. Thus a surface correlation function can be approximated by plotting this peak value versus the insonified area separation.

assuming e_1 to be directed along R_1. The bracketed term ({...}) is just the pressure field scattered from a plane surface corresponding to the image solution P_R, which is evaluated with a stationary phase integral. The term $\langle \exp[-ik\gamma\zeta] \rangle$ represents the Fourier transform (FT) of the PDF of surface heights or the characteristic function (CF).

C. Covariance of Scattered Pressure

The covariance of the pressure field can be derived with a simplification of Eq. II.17. Since we have already assumed a sufficiently directional source, we can write Eq. II.17 as

$$P_S(r) = [ik/(2\pi)] \int\int D_0(x,y) \ (\{\exp[ik(r+s)]\}/[rs]) \ \exp[-ik\gamma\zeta]$$

$$\times [\zeta_x e_x + \zeta_y e_y + e_z] \cdot e_1 \ dx \ dy \quad , \qquad\qquad II.24$$

where $r=|r|$ and $s=|s|$. If we assume that the slopes are negligible the covariance of the pressure becomes

$$\langle P_S(r) \ P_S(r')^* \rangle = \langle \exp[ik(\gamma\zeta - \gamma'\zeta')] \rangle \ [k/(2\pi rs)]^2$$

$$\times \int\int\int\int D_0(x,y) \ D_0(x,y)^* \ (e_z \cdot e_1)(e_z \cdot e_1') \ dx \ dy \ dx' \ dy' \quad . \qquad II.25$$

However, the integral does not simplify much further (but can be evaluated numerically) and at this point it is necessary to reflect upon the work of Reference 18 and the results relating the covariance to the correlation function of the surface.

quantities we will be concerned with are the so-called mean scattered pressure and the covariance of the pressure field.

B. Mean Scattered Pressure

The ensemble average of the pressure field, or mean scattered pressure, expressed in Eq. II.17 is defined with

$$\langle P_s \rangle = \iiint P_s \, \omega(\zeta,\zeta_x,\zeta_y) \, d\zeta \, d\zeta_x \, d\zeta_y \qquad\qquad \text{II.18}$$

for ω, the three-dimensional probability density function (PDF) of surface heights and slopes. The ensemble average represents the average over the variation of the total area insonified on the surface. For a time varying surface (ζ a function of time) this is a time average, and for a fixed surface (ζ a function of x and y) this is an average over a number of insonified surface areas. If ζ, ζ_x, and ζ_y are uncorrelated, then Eq. II.17 becomes

$$\langle P_s(r) \rangle = [ik/(2\pi)] \iint D_0(x,y) \, (\{\exp[ik(R_0+R_1)]\}/[R_0 \, R_1]) \, \langle \exp[-ik\gamma\zeta] \rangle$$

$$\times \langle [\zeta_x e_x + \zeta_y e_y + e_z] \cdot e_1 \rangle \, dx \, dy \quad , \qquad\qquad \text{II.19}$$

and with the ζ_x and ζ_y zero mean processes,

$$\langle P_s(r) \rangle = \langle \exp[-ik\gamma\zeta] \rangle \, \{[ik/(2\pi)] \iint D_0(x,y) \, (\{\exp[ik(R_0+R_1)]\}/[R_0 \, R_1])$$

$$\times \sin \theta_r \, dx \, dy\} \quad , \qquad\qquad \text{II.20}$$

10

and for a source concentrating the incident energy within a small region about the directional axis (a directional source of finite beamwidth),

$$\sin \psi_0 \approx \sin \theta_i \quad \text{and} \quad \sin \psi_1 \approx \sin \theta_r \quad . \qquad \text{II.15}$$

Approximations for r_0 and r_1 then follow:

$$r_0 \approx R_0 - \zeta \sin \theta_i \quad \text{and} \quad r_1 \approx R_1 - \zeta \sin \theta_r \quad . \qquad \text{II.16}$$

Now the exponential in Eq. II.13 is greatly simplified and can be broken down into a term dependent upon the plane surface geometry and a term dependent upon the surface heights. Also it should be noted that the denominator $r_0 r_1$ varies slowly with respect to the exponential and can be replaced with $R_0 R_1$. Therefore, for receiver points far from the surface and near normal incidence (with negligible shadowing) Eq. II.13 becomes

$$P_S(r) = [ik/(2\pi)] \int\!\!\int D_0(x,y) \, (\{\exp[ik(R_0+R_1)]\}/[R_0 \, R_1]) \, \exp[-ik\gamma\zeta]$$

$$\times [\zeta_x e_x + \zeta_y e_y + e_z] \cdot e_1 \, dx \, dy \qquad \text{II.17}$$

for $\gamma = \sin \theta_i + \sin \theta_r$.

Suppose that the surface heights $\zeta(x,y)$ can be described with a two-dimensional zero mean random variable. This allows us to define various statistical properties of the pressure field. The two particular

$$(\delta/\delta n)\ ([\exp(ikr_1)]/r_1) = ik(\mathbf{n}\cdot\mathbf{e}_1)\ ([\exp(ikr_1)]/r_1) \quad . \tag{II.10}$$

Also, an expression for the unit normal vector and surface element can be derived using differential geometry,

$$\mathbf{n} = \nabla\zeta/|\nabla\zeta| = [\zeta_x\mathbf{e}_x + \zeta_y\mathbf{e}_y + \mathbf{e}_z]/\sqrt{[(\zeta_x)^2 + (\zeta_y)^2 + 1]} \tag{II.11}$$

and

$$d\Sigma = \sqrt{[(\zeta_x)^2 + (\zeta_y)^2 + 1]}\ dx\ dy \quad , \tag{II.12}$$

where ∇ is the differential operator, ζ_x and ζ_y are the surface slopes with respect to x and y, and $\mathbf{e}_x$, $\mathbf{e}_y$, and $\mathbf{e}_z$ are the Cartesian coordinate system unit vectors.

Equation II.6 now becomes

$$P_S(\mathbf{r}) = [ik/(2\pi)]\iint D_0(x,y)\ (\{\exp[ik(r_0+r_1)]\}/[r_0\ r_1])$$

$$\times[\zeta_x\mathbf{e}_x + \zeta_y\mathbf{e}_y + \mathbf{e}_z]\cdot\mathbf{e}_1\ dx\ dy \quad . \tag{II.13}$$

According to Spetner,[25] the surface roughness is assumed smaller than both the source and receiver distances, or

$$(2\zeta/R_0)\sin\psi_0 \ll 1 \quad \text{and} \quad (2\zeta/R_1)\sin\psi_1 \ll 1 \quad , \tag{II.14}$$

another result is that multiple scattering and shadowing are neglected.

From Eq. II.5, the Green's function solution simplifies to

$$P_S(r) = [1/(2\pi)] \iint P_i(r_S) \{(\delta/\delta n) ([\exp(ikr_1)]/r_1)\} \, d\Sigma \quad . \qquad \text{II.6}$$

For a directional acoustic source emitting spherically radiating wavefronts, the incident pressure is

$$P_i = D_0(x,y) \, ([\exp(ikr_0)]/r_0) \qquad \text{II.7}$$

in the farfield, where D_0 is the pressure density proportional to the directivity pattern of the source and r_0 the distance from $d\Sigma$ to the source.

The partial derivative of the integrand in Eq. II.6 can be evaluated as

$$(\delta/\delta n) ([\exp(ikr_1)]/r_1) = ik(n \cdot e_1) (1-[1/(ikr_1)]) \, ([\exp(ikr_1)]/r_1) \qquad \text{II.8}$$

for a unit normal vector n pointing into the surface and e_1 a unit vector pointing along r_1. At this point, the Fresnel-Kirchhoff approximation can be easily applied such that

$$kr_1 \gg 1 \quad , \qquad \text{II.9}$$

which is equivalent to assuming that the observation range is longer than the wavelength of the source. Equation II.8 then becomes

7

The scattered pressure P_S satisfies the wave equation

$$\{\nabla^2 + k^2\} P_S = 0 \quad , \qquad\qquad II.2$$

where ∇^2 is the Laplacian operator and $k=2\pi/\lambda$ is the wave number for wavelength λ. A solution to Eq. II.2 is

$$P_S(r) = [1/(4\pi)] \int\int P_i(r_S) \{(\delta/\delta n) G(r,r_S)\} d\Sigma \quad , \qquad II.3$$

where P_i is the incident pressure, $(\delta/\delta n)$ the partial derivative with respect to the normal to the surface n, $d\Sigma$ the surface element, and G the Green's function which satisfies

$$\{\nabla^2 + k^2\} G = -4\pi \delta(r - r_S) \qquad\qquad II.4$$

for G vanishing on the surface.[23] The observation point is at r with $d\Sigma$ at r_S. However, for an irregular surface, G is rather hard to evaluate. But for a plane surface placed tangentially to $d\Sigma$, G is well known,[24] and

$$\{(\delta/\delta n) G\} = 2 \{(\delta/\delta n) ([\exp(ikr_1)]/r_1)\} \qquad\qquad II.5$$

for r_1, the distance from $d\Sigma$ to the receiver. This means that the radius of curvature of the roughness is assumed much greater than the wavelength;

6
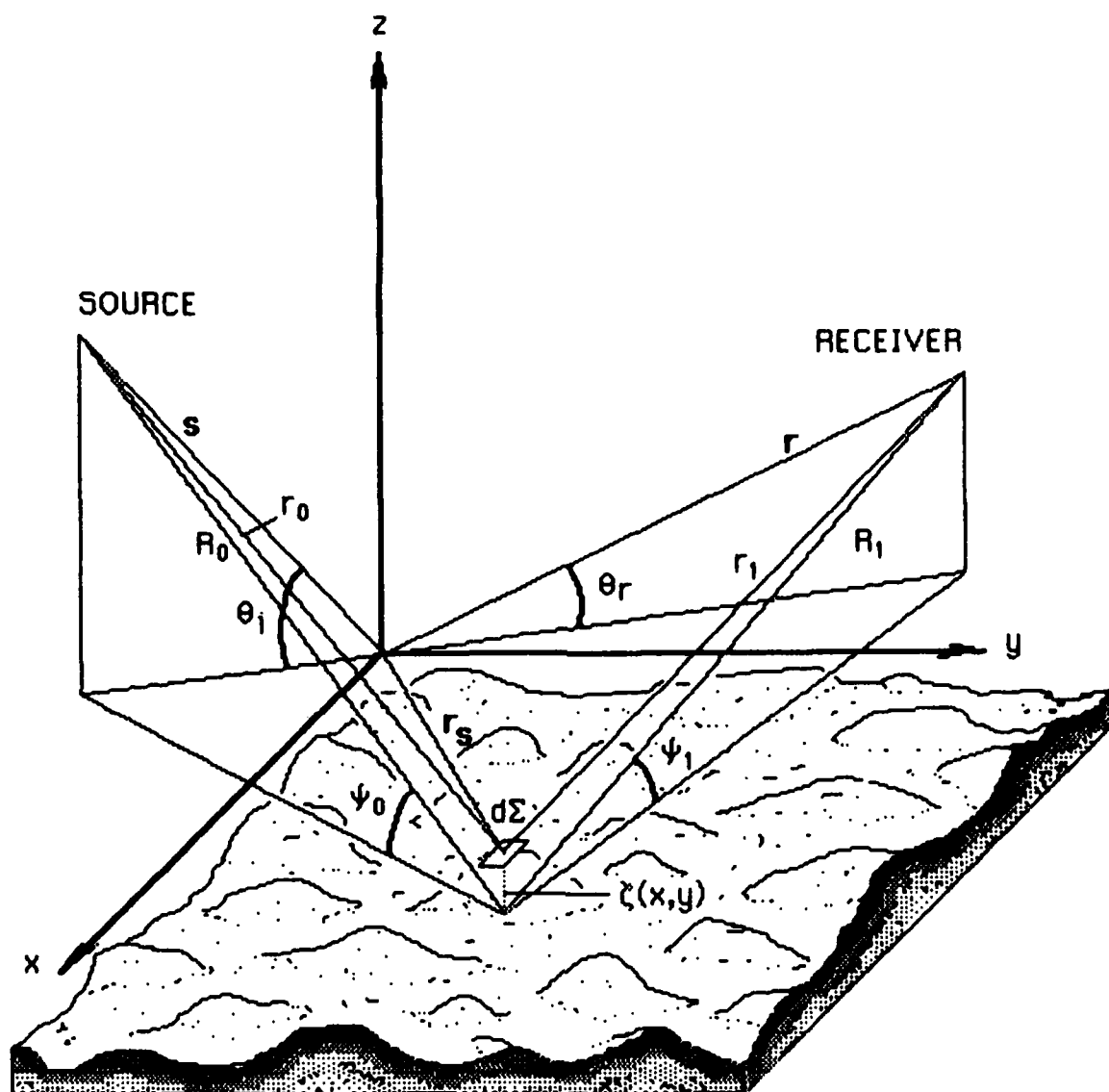
FIGURE 1
COORDINATE SYSTEM AND GEOMETRY FOR ROUGH SURFACE SCATTERING

II. ACOUSTIC THEORY

This section describes the acoustic theory which leads to the formulation of the inverse problem. The mathematical framework of the forward problem provides the context for solution of the inverse problem. The physical model established by Eckart is used as the foundation for the inverse theory. The development used here follows very closely that of Clay and Medwin[18] and Boyd and Deavenport.[14] An expression for the pressure field scattered from rough surfaces is derived which can be sii.iplified with knowledge of the incident pressure field and the assumption of a randomly rough interface.

A. Eckart's Scattering Theory

Consider the scattering geometry of Fig. 1; the source is spherically divergent, with position vector s incident upon the surface Σ, and the receiver is at r. With the surface height defined by the variable $\zeta(x,y)$ (in the direction of the z axis) , the coordinate system is oriented such that the x-y plane lies in the average surface height described by

$$\iint \zeta(x,y)\ dx\ dy = 0 \qquad\qquad \text{II.1}$$

and the origin is the point where the beam axis of the source, assumed directional, intersects the mean plane.

$v(\zeta)$ is the DFT of the characteristic function, and the $S^{(1)}_{0j}$ are the prolate angular wave functions of the first kind.

Convergence of the summation depends upon many factors. The DFT is discrete and thus the inner product will be represented by a numerical integral introducing numerical error due to the integral approximation. The value ζ_{max} represents an estimate of the bound on the surface heights, and so knowledge of the maximum surface height is necessary. The $S^{(1)}_{0j}$ are more oscillatory as the index j increases and as the product $2\pi\xi_m\zeta_{max}$ approaches infinity. As a result most of the contribution to the summation will be due to the lower order $S^{(1)}_{0j}$. Also, if errors in the original characteristic function exist, then the errors in the summation will also be large. In general, Perry[29] shows that the BL technique is numerically unstable for certain cases. The degree of instability depends upon the value $2\pi\xi_m$; the smaller this value is, then the more stable the method is.

3. Extended Prony Method

Another high resolution spectral estimator which has been used is the extended Prony method (EP),[30] known for its ability to accurately predict the Fourier spectra of short data records. The Prony method has been used in spectral estimation, data reconstruction, and resonance extraction from transient response functions. The Prony method, presented in detail in Appendix B, consists of expanding a complex function known at evenly sampled sub-intervals with a basis set of complex exponentials. This expansion can be expressed as

18

$$\Omega(\xi) = \sum_{j=1}^{q} c_j \exp[s_j \xi] \qquad \text{III.8}$$

or, for discrete values of $\xi = \ell \Delta \xi$,

$$\Omega(\ell \xi) = \sum_{j=1}^{q} c_j [z_j]^\ell \quad , \quad \ell = 0,...,M-1 \qquad \text{III.9}$$

which looks similar to the DFT expansion of Eq. III.4. However, the $\{s_j\}$ are complex in general and non-harmonically related,

$$s_j = \alpha_j + i2\pi\zeta_j \qquad \text{III.10}$$

and

$$z_j = \exp[s_j \Delta \xi] \quad , \qquad \text{III.11}$$

where the α_j is a damping factor. Unlike in the DFT, no assumptions about periodicity are made but instead all parameters are estimated including the complex frequencies, s_j, and complex amplitudes, c_j. The frequencies of

19

the spectra are not predetermined by the choice of data record length nor is the process restricted to cosines and sines. If it is also assumed that

$$c_j = A_j \exp[i\theta_j] \quad , \tag{III.12}$$

are complex amplitudes, then the FT of Eq. III.25 is

$$\omega(\zeta) = \sum_{j=1}^{q} c_j \, 2\alpha_j / [\alpha_j^2 + \{2\pi(\zeta - \zeta_j)\}^2] \quad . \tag{III.13}$$

The data are first assumed to follow linear prediction models so that a linear Toeplitz system of equations,

$$\Omega(\ell) = \sum_{j=1}^{q} a_j \, \Omega(\ell-j) \, , \, \ell = q, \dots , M-1 \quad , \tag{III.14}$$

can be solved for the prediction coefficients such that $a_0 = -1$. The equation

$$\sum_{j=0}^{q} a_j \, z^{(q-j)} = 0 \tag{III.15}$$

is a polynomial equation which can be solved for the damping factors and frequencies z_j. The complex amplitudes are then retrieved from a solution to a Vandermonde system of equations in Eq. III.9. The Fourier spectrum of Eq. III.13 is then calculated as an estimate of the PDF.

One problem associated with implementing the extended Prony method is the determination of the number of estimation parameters q. A method for doing this is presented in Appendix B. Noise also affects the accuracy of the EP method, the largest impact being on the damping factors $\{\alpha_j\}$ which become larger with lower signal-to-noise ratios.

B. Correlation Function

The correlation function can be obtained from the covariance of the pressure of Section II.C. The correlation function describes the correlation of the surface profile, i.e., how much one portion of the surface compares quantitatively with another portion a distance away.

However, the discussion of the correlation function differs from the PDF discussion in that the Fourier transform domain consists of spatial position and spatial wave number space, as opposed to the surface heights/surface wave number space for the PDF.

Following the definition of the DFT given by Eqs. III.4 and III.5, the following DFT pair involving the spatial pressure field is also observed,

$$P(\ell r) = \Delta\rho \sum_{j=0}^{M-1} p(j\rho) \exp[-i2\pi\ell j/M] \ , \ \ell = 0, \ldots , M-1 \qquad \text{III.16}$$

21

and

$$p(j\rho) = \Delta r \left[\sum_{\ell=0}^{M-1} P^*(\ell r) \exp[-i2\pi\ell j/M] \right]^* \quad , j = 0, \dots, M-1 \quad , \qquad \text{III.17}$$

where $P(\ell r)$ represents the sampled version of the pressure field with the uniform sampling increment (in Cartesian coordinate space) of Δr (instead of surface wave number space).

An estimate of the covariance of the pressure field in Eq. II.25 is possible with the inverse FT of the cross-power spectrum[31] of the pressure, or

$$R_\delta(\ell\epsilon) = \Delta\rho \sum_{j=0}^{M-1} s_\delta(j\rho)^* \exp[-i2\pi\ell j/M] \quad , \ell = 0, \dots, M-1 \quad , \qquad \text{III.18}$$

where the covariance is assumed to be a function of the spatial separation of the positions $\epsilon = |r-r'|$. The cross-power spectrum is defined

$$s_\delta(j\rho) = \langle p_0(j\rho) \, p_\delta(j\rho)^* \rangle \quad , \qquad \text{III.19}$$

where the p's are the FT's of the pressure fields from spots 0 and δ, respectively (insonified spots being separated by a distance of δ).

22

An estimate of the correlation function of the surface is possible by calculating the covariance of all spatial pressure field pairs (p_0's and p_δ's) associated with various surface spot separations. The resulting covariance can be normalized with the autocovariance measurements at $\epsilon = 0$, or

$$A_0 = \Delta\rho \sum_{j=0}^{M-1} \langle |p_0(j\rho)| \rangle \qquad \text{III.20}$$

and

$$A_\delta = \Delta\rho \sum_{j=0}^{M-1} \langle |p_\delta(j\rho)| \rangle \quad . \qquad \text{III.21}$$

which yields the normalized correlation function

$$C_\delta(j\epsilon) = R_\delta(j\epsilon)/\sqrt{(A_0 A_\delta)} \quad . \qquad \text{III.22}$$

The correlation will have a peak value at some delayed value of ϵ due to the separation of the spots δ. The correlation of the surface can be constructed by noting the peak values of C at these delayed ϵ values and plotting them versus the spot separation δ. This is verified with actual experimental data in Appendix C.

23

IV. EXPERIMENT AND DATA ACQUISITION

The subjects of Chapters II and III were the development of the acoustical inverse theory which would allow inference of the statistical properties of the scattering surface, the rms height, and the correlation length. This chapter describes the experiment which is used to verify this theory. First, the constraints involved in the theoretical development that are most critical in the experimental arrangement are outlined, followed by a discussion of the specific experimental parameters used.

A. Considerations

Before the theory can be assessed, a valid experiment must first be designed with the assumptions of the theoretical development in mind. The choice of a rough surface model was the first consideration. Three pressure release polystyrene models (82 cm by 82 cm) constructed from aeromagnetic maps of the Canadian Shield[22] were used and the statistical properties of the surfaces are well known (see Fig. 4). An actual histogram of heights (PDF) of surface 3 (also representing surfaces 1 and 2 with appropriate scale changes) was developed by measuring the heights of 1089 points on the surface (Fig. 2). Figure 3 represents the autocorrelation function of the surface for two perpendicular orientations of the surface. A Gaussian and exponential curve have been fit to both the histogram and correlation function, respectively. A measure of the rms height is obtained

24
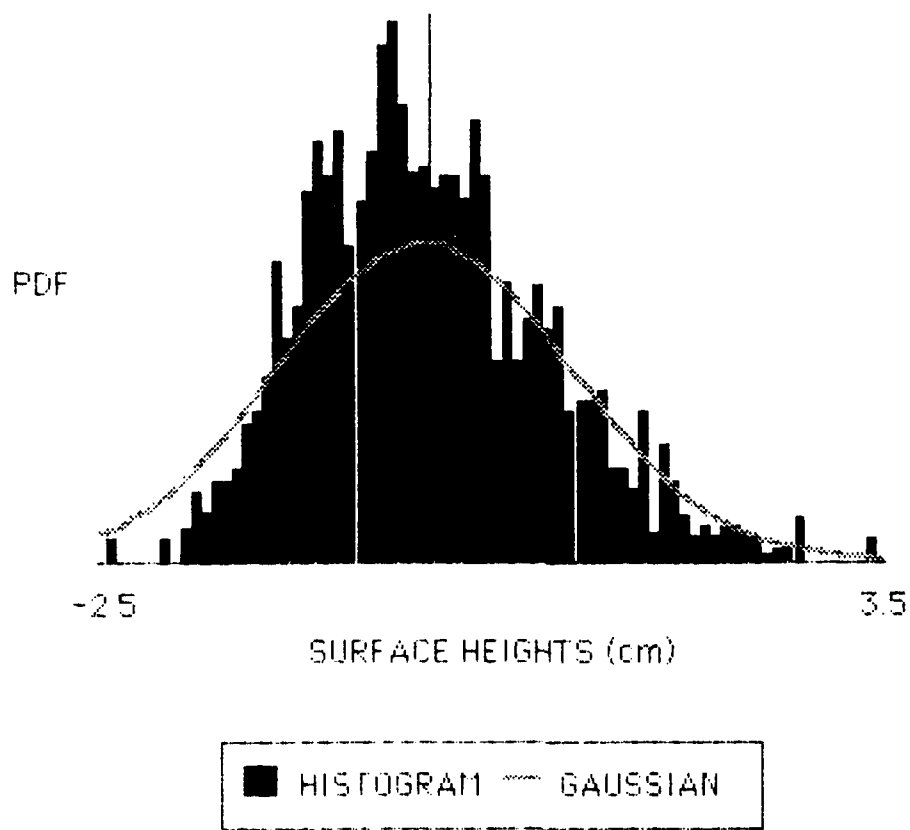
FIGURE 2
HISTOGRAM OF HEIGHTS MEASURED AT 1089 POINTS IN THE CENTRAL
QUARTER OF THE THIRD ROUGH SURFACE (COURTESY OF S. K. MITCHELL)
STANDARD DEVIATION OF THE GAUSSIAN CURVE IS 1.13 cm, WHICH
APPROXIMATES THE rms HEIGHT OF THE SURFACE

AS-85-308
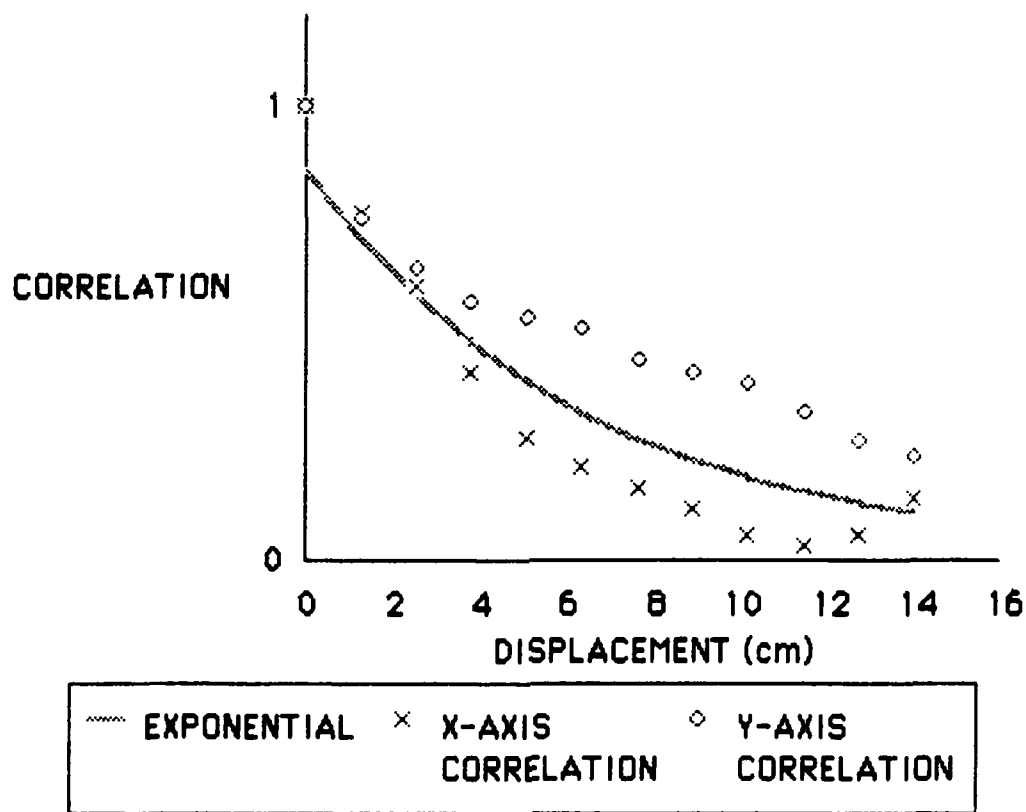
FIGURE 3
AUTOCORRELATION OF THE SURFACE MEASURED FROM THE CENTRAL
QUARTER OF THE THIRD MODEL SURFACE (COURTESY OF S. K. MITCHELL)
THE E-FOLDING VALUE OF THE EXPONENTIAL CURVE IS 4.51 cm, WHICH
APPROXIMATES THE CORRELATION LENGTH OF THE SURFACE

26

with the standard deviation of the Gaussian function, and a measure of the correlation length is obtained by observing the e-folding (1/e) point of the exponential function.

The next consideration was that of establishing an acoustic measurement geometry. Recall that the acoustic source is restricted to near-normal incidence so that there will be a minimum shadowing of the surface. Shadowing studies[32] were conducted on the first three rough surfaces and estimates of the shadowing functions obtained. A choice of $\theta_i > 50°$, such that the shadowing function is unity, will assure that shadowing is insignificant. Figure 4 represents the experimental geometry and is referenced for the rest of the discussion.

The wavelength of the incident acoustic pressure must also be selected. A rough guide to this choice is the Rayleigh criterion[10] of surface roughness. A surface is considered effectively smooth if

$$\zeta_{rms}/\lambda \to 0 \quad \text{or} \quad \theta_i \to 0 \quad , \qquad\qquad \text{IV.1}$$

which should set an upper limit on λ. Another guide to the choice is to select a range on ζ for sampling the main structure of the characteristic function. If a Gaussian PDF is assumed, the use of the $3\zeta_{rms}$ point of the characteristic function yields a lower limit on λ, or

$$3/\zeta_{rms} > (\sin\theta_i + \sin\theta_r)/\lambda \quad . \qquad\qquad \text{IV.2}$$

27
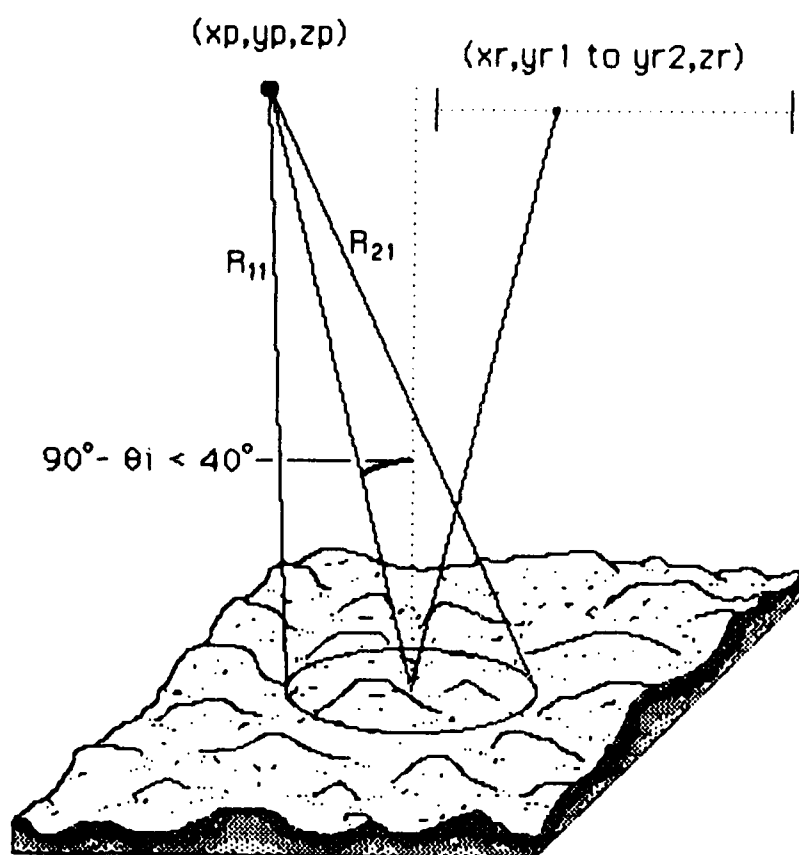
Model	1	2	3
rms Height, ζ_{rms}	0.231 cm	0.462 cm	0.924 cm
Correlation length	6.48 cm	6.48 cm	6.48 cm
Wavelength, λ	1.88 cm	1.88 cm	1.88 cm
Transmit, (xp,yp,zp)	(0,-50,275)	(0,-50,275)	(2,-70,293)
Receive, (xr,yr1;yr2,zr)	(0,27;73,275)	(0,27;73,275)	(-31,-1;121,273)
Spot radius, a≈b	16.5 cm	16.5 cm	16.5 cm
Number of spots	49	49	69
Transmit pulsewidth	450 μs	450 μs	600 μs
Repetition rate	25 /s	25 /s	30 /s
Receive pulsewidth	125 μs	125 μs	200 μs

FIGURE 4
EXPERIMENTAL GEOMETRY AND PARAMETERS

28

AS-85-310

The solutions are valid for directional sources only so a fairly small beamwidth is necessary. This parameter is of particular interest since the beamwidth along with the range will determine the illumination spot size on the surface and the number of independent spots which can be insonified. The larger the number of spots, the larger will be the ensemble over which the mean scattered pressure is calculated in Eq. II.20. Also, the dimension of the spots should be on the order of a correlation length so that at least one correlation length of the surface is insonified.

The insonified area on the surface is considered to be determined by the -3 dB beamwidth (β) contour. For a directional source beam pattern which exhibits azimuthal symmetry, the spot is elliptical with semi-major axis a and semi-minor axis b,

$$a = z_p \tan(\beta/2)/\sin^2\theta_i \qquad\qquad IV.3$$

and

$$b = a \sin\theta_i \qquad\qquad IV.4$$

where z_p is the range, being determined by the farfield distance of the source, or $z_p > S/\lambda$ for S, the acoustically active surface area of the source.

The orientation of the source and receiver should also be such that the source does not interfere with the measurements of the field. So restricting the measurements to the -10 dB contour will yield an elliptical

29

spot of $2\sqrt{(10/3)}$ times that of the surface spot. This will also prevent the characteristic function from being undefined as the image solution approaches zero.

Also, a time T_i is required to illuminate the surface within the -3 dB contour. From Fig. 4 it is noted that

$$R_{11} = yp/\sin(\theta_i + \beta/2) \quad , \qquad \qquad \text{IV.5}$$

$$R_{21} = yp/\sin(\theta_i - \beta/2) \quad , \qquad \qquad \text{IV.6}$$

and

$$T_i = (R_{21} - R_{11})/c \quad , \qquad \qquad \text{IV.7}$$

where c is the sound speed in water (1500 m/sec). This time delay results in a rise time that will allow a pulsed signal to be detected as a steady state signal. There is also a time delay T_d between transmit at the source and receive at the receiver, or

$$T_d = (R_{21} + R_{11})/c \quad . \qquad \qquad \text{IV.8}$$

The experimental measurements were done in a sonar model tank room, which meant that there would be multiple reflections due to the walls, water surface, and tank bottom. This problem was overcome by

30

operating the source in a pulsed mode rather than a continuous mode so that a particular pulse rate and pulse width can be selected such that the reflections will not interfere with the return pulse from the rough surface. Thus, the timing involved in obtaining the scattered pressure measurements is critical in that the proper delay of the observation interval should be chosen to capture the valid scattering.

It is impractical (if not impossible) to experimentally measure the characteristic function for all possible surface wave numbers. However, we can obtain a finite number of discrete values. According to the sampling theorem he characteristic function must be sampled at least at the Nyquist rate in even intervals of the variable ζ. Thus the receiver and source positions or wavelengths must be selected such that ζ is incremented in even intervals. This is done by maintaining the source as stationary (θ_i fixed), radiating one frequency (λ fixed), and moving the receiver (θ_r varied) such that Ω is sampled in even increments. The covariance function requires the sampling of the pressure field in even increments of space, so a technique must be developed to allow sampling both in space and surface wave number space, ζ.

B. Geometry and Experimental Equipment

The forward scattered data were collected in the sonar model tank room at ARL:UT. The scattering surfaces were a plane pressure release surface and three randomly rough surfaces constructed specifically for scattering studies. The complex pressure field was measured using a line and cone transducer[33] as the narrowbeam projector and an H-56 standard

31
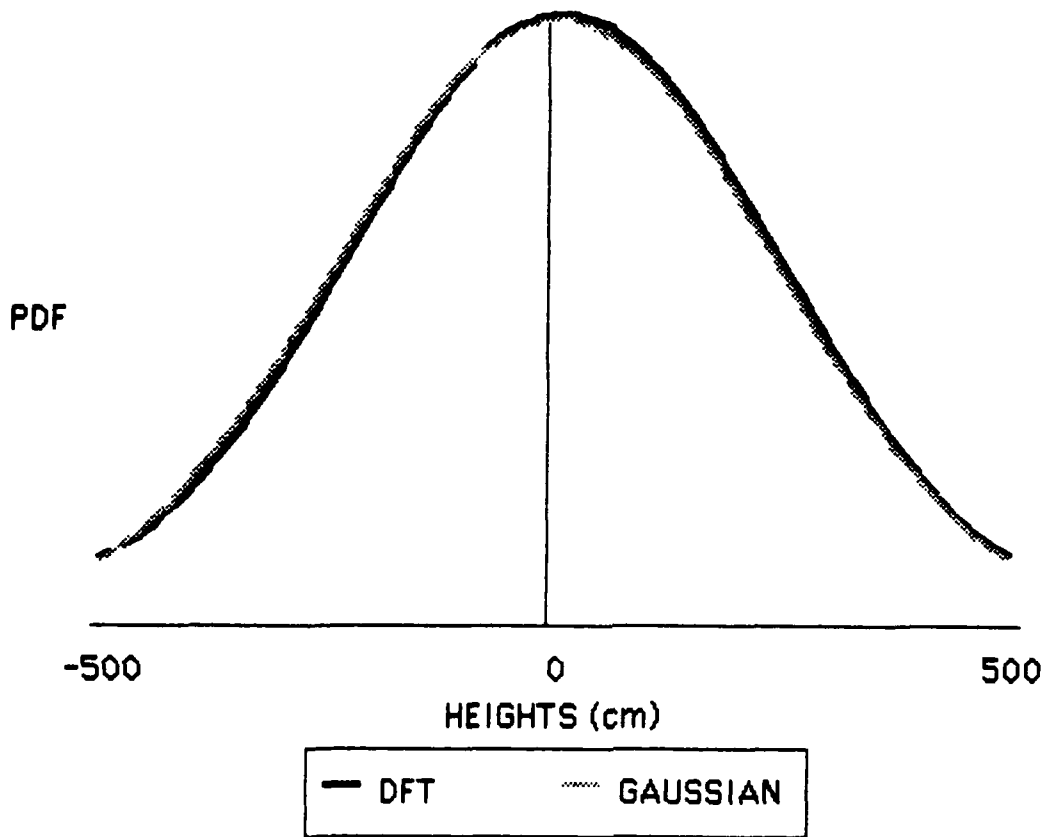
FIGURE 10
THE PROBABILITY DENSITY FUNCTION FOR THE SECOND ROUGH
SURFACE VIA THE DISCRETE FOURIER TRANSFORM TECHNIQUE
STANDARD DEVIATION OF THE GAUSSIAN CURVE IS 237 cm

45

AS-85-316
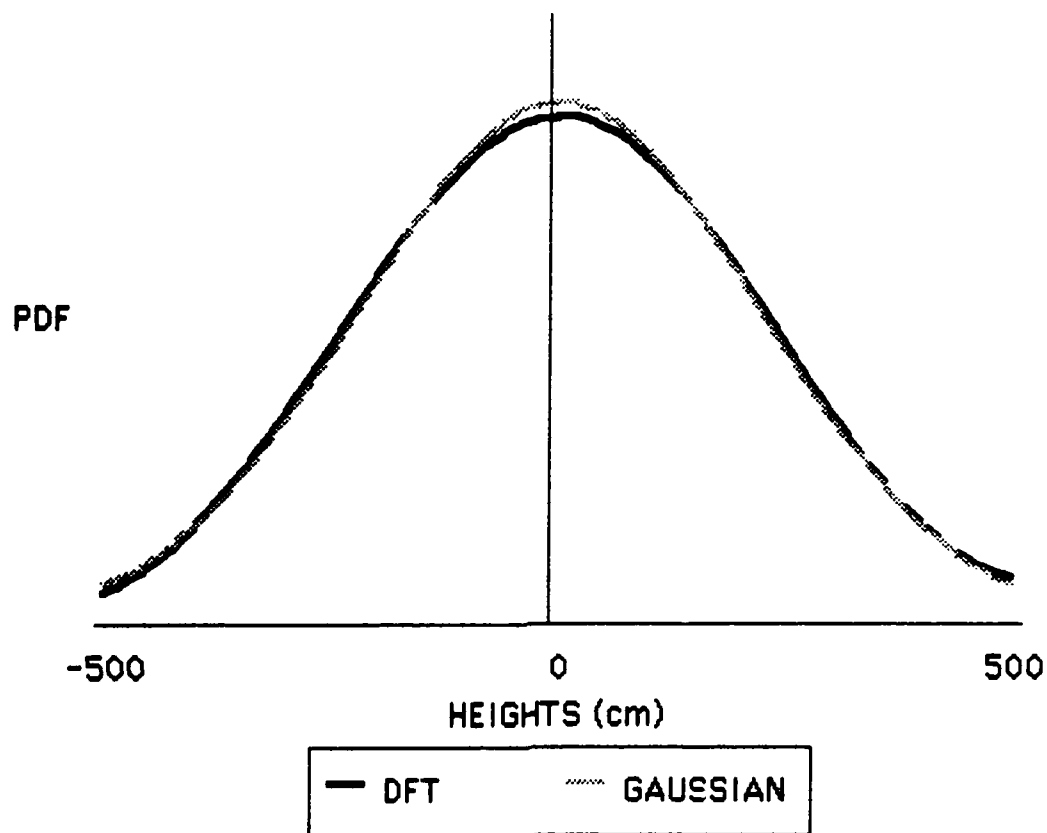
FIGURE 9
THE PROBABILITY DENSITY FUNCTION FOR THE FIRST ROUGH
SURFACE VIA THE DISCRETE FOURIER TRANSFORM TECHNIQUE
STANDARD DEVIATION OF THE GAUSSIAN CURVE IS 219 cm

AS-85-315

rms Height (in cm)

Surface	Actual	DFT	Elementary Bandwidth	BLM	EPM
1	.231	219	214	71.4	32.7
2	.462	237	214	82.5	41.2
3	.924	47.0	22.4	8.81	1.40

Correlation Length (in cm)

Surface	Actual	Calculated	Spatial Lag	Spot Separation Increment
1	6.48	7.03	.55	3.18
2	6.48	3.32	.55	3.18
3	6.48	5.18	.55	2.29

TABLE I: Summary of results of the estimates of rms height and correlation length

43

the Gaussian curve, carefully noting the degree of goodness of fit between the estimates and analytical curve. For more realistic comparisons, however, the structure about the central maximum must also be fitted with a Gaussian curve.

The accuracy of the rms height estimates is a problem due to the finite extent of the observation window. The elementary bandwidth is the inverse of the observation window and is directly related to the resolution of the Fourier transform estimate. Thus, the length of the data observation window will affect each of the three techniques and resolution will improve as the observation window is increased. Also, greater resolution is achieved with EPM than with BLM, and better resolution with BLM than DFT. All three methods are somewhat sensitive to changes in the rms height when the observation window is the same, as seen in comparisons of the PDF estimates of surfaces 1 and 2. These results are summarized in Table I, the values representing the estimated rms heights obtained from Gaussian curves fitted to the PDF estimates of the three techniques.

1. DFT Technique

Figures 9, 10, and 11 represent the discrete Fourier transform technique applied to the characteristic functions of surfaces 1, 2, and 3, respectively. These results will be the benchmark by which the other two techniques are compared for resolution. For surfaces 1 and 2, the elementary bandwidth of the surface heights is 214 cm when the observed data record is used by itself. However, this resolution of heights can be

42

least means square solution for the $\{c_j\}$ in Eq. III.9. The Fourier spectrum is then computed with application of Eq. III.13, and as in the Bojarsky-Lewis method, extrapolation or interpolation of the characteristic function is possible.

The correlation function computation proceeds with the FFTs of the scattered pressure fields from each of the spots (Eq. III.17). Since the correlation function estimate is valid for zero-mean stochastic processes,[31] the mean value of the pressure must be zero before proceeding. The auto-power and cross-power spectra of the pressure fields corresponding with spots separated a given distance are then computed with Eq. III.19, the ensemble average being the average over the ensemble of spot pairs. The normalized correlation function (Eq. III.22) for each possible spot separation is computed via the inverse FFT and with knowledge of the zero-lag values of the auto-power spectra (Eqs. III.20 and III.21). The peak value of the correlation is then plotted versus the spot separation of the spots.

B. PDF Estimates

This section presents the numerical solutions resulting from the application of the three PDF estimation techniques upon the experimental data. The results are presented for each of the three model rough surfaces. The general structure of the PDFs is bounded and Gaussian in shape. Therefore, a Gaussian function is fit to the PDF estimates to minimize the mean squared error between the Gaussian and the estimate (a least mean square fit). The rms height value is taken to be the standard deviation of

41

the fast Fourier transform (FFT) algorithm.[27]

For the application of the Bojarsky-Lewis method, the prolate angular wave functions must be calculated for use in Eq. III.6. These functions are calculated with knowledge of ξ_m and ζ_{max} and the algorithm of Reference 36. The value used for ξ_m is the average value of the surface wave number over the range of sampling of the characteristic function, and the value used for ζ_{max} is an estimate of the bound on the surface heights. This value is assumed to be three times the actual rms surface height of the model surface. Recalling the truncated summation of Eq. III.6, one notes the inner product between the prolate angular wave functions and the estimate of the PDF, $v(\zeta)$ of Eq. III.7. The estimate of v is computed with the FFT of Eq. III.5 as in the discrete Fourier transform technique above (however, no optimal window is applied). The inner product is then calculated as a numerical integral. Due to the continuous nature of the estimate of Eq. III.6, any interpolated or extrapolated value for the PDF is possible, the only limitation being the truncation of the summation.

As in the Bojarsky-Lewis method, the extended Prony method is a multiple step process. The sampled characteristic function forms the data vectors of Eq. B.11 for calculation of the data matrix of Eq. B.17, thus requiring knowledge of the value for q. The eigenvalue decomposition of the matrix is computed and the weakest eigenvector (corresponding to the smallest eigenvalue) is the vector of Eq. B.18. The polynomial of Eq. III.15 is then rooted to find the values for the $\{z_j\}$, which are then used to find a

40

pressure corresponds to the -3 dB beamwidth of the image solution. The scattering from surface 3 is observed over the -10 dB beamwidth of the image solution. This data observation length determines the resolution of the PDF estimates, as will be seen.

The plots were digitized so that data points could be interpolated for sampling the pressure in even increments of both surface wave number space (ξ) and Cartesian coordinate space (r). A "cubic spline" technique (fitting a cubic equation to data points) was used for interpolation of the digitized amplitude and a linear interpolation method was used for the digitized phase.

The uniform sampling in surface wave number space allows the calculation of the PDF and the sampling in coordinate space allows the calculation of the correlation function. Thus, following interpolation, solutions to the inverse problem can be sought. For the calculation of the PDF, the characteristic function must be computed using Eq. III.1. The numerator is the mean scattered pressure and is calculated with the ensemble average of the pressure field over the independently insonified spots. The image solution is the pressure field for the reflection from the planar surface. The inverse Fourier transform of the characteristic function must now be estimated with one of the three techniques of Chapter III.

Before the application of the discrete Fourier transform, an optimal window, the Kaiser-Bessel window,[28] is applied to the characteristic function. The discrete Fourier transform of Eq. III.5 is then applied using
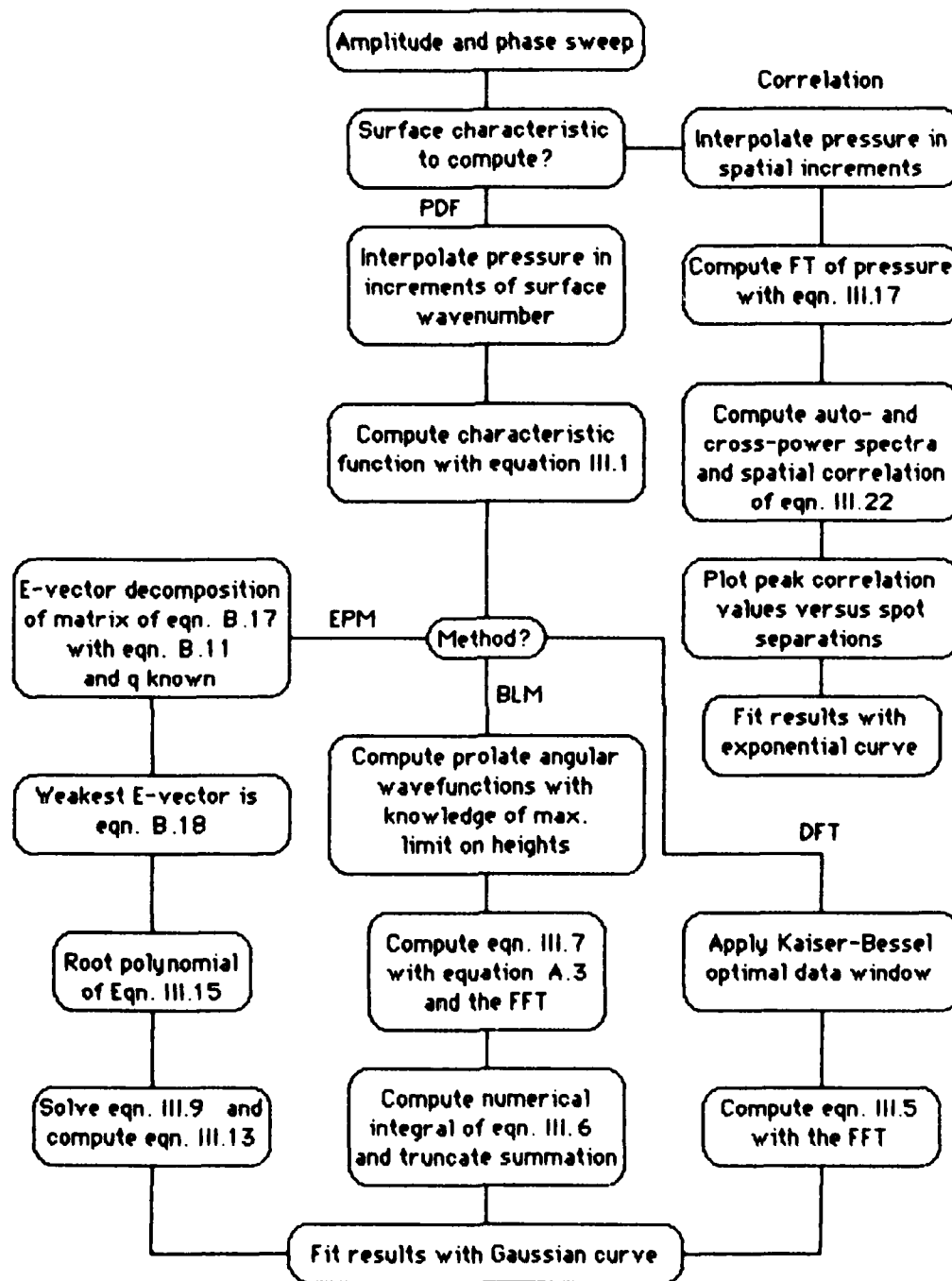
39

FIGURE 8
FLOWCHART OF THE PROCESSING OF THE SCATTERED PRESSURE
DATA FOR INFERENCE OF THE PDF AND CORRELATION FUNCTION

38

AS-85-314

V. RESULTS

This chapter describes the analysis of the scattered pressure field measurements using the processing techniques discussed in Chapter III. The numerical results of the calculations for each of the model rough surfaces are presented and compared with the actual statistical parameters of the model surfaces. Suggestions are made for improving the accuracy of the results where appropriate.

A. Data Processing

The implementation of the signal processing techniques in Chapter III is straightforward, in that the equations necessary for the processing are all present in the text. Figure 8 is a flowchart of these processing techniques, which were programmed in FORTRAN for use on a CYBER 171 digital computer available at ARL:UT. Although the actual coding is not presented here, archived copies of the programs along with documentation for usage are available upon request.

The complex pressure field measurements are represented with the amplitude and phase sweeps obtained from the receiving hydrophone (the output of the voltmeter and phasemeter[35]). The scattered pressure field from both the planar surface and the model surface are necessary to compute the PDF, the scattering from the plane surface being used as the image solution. For surfaces 1 and 2, the observation interval of the

FIGURE 7
A SAMPLE PHASE PLOT OF THE OUTPUT OF THE PHASEMETER versus THE
SPATIAL POSITION OF THE HYDROPHONE
THE SAMPLING INCREMENT IS UNIFORM IN CARTESIAN COORDINATE SPACE
THIS REPRESENTS THE PHASE OF THE PRESSURE FIELD OF THE SCATTERING
FROM ONE INSONIFIED SURFACE SPOT ON SURFACE THREE

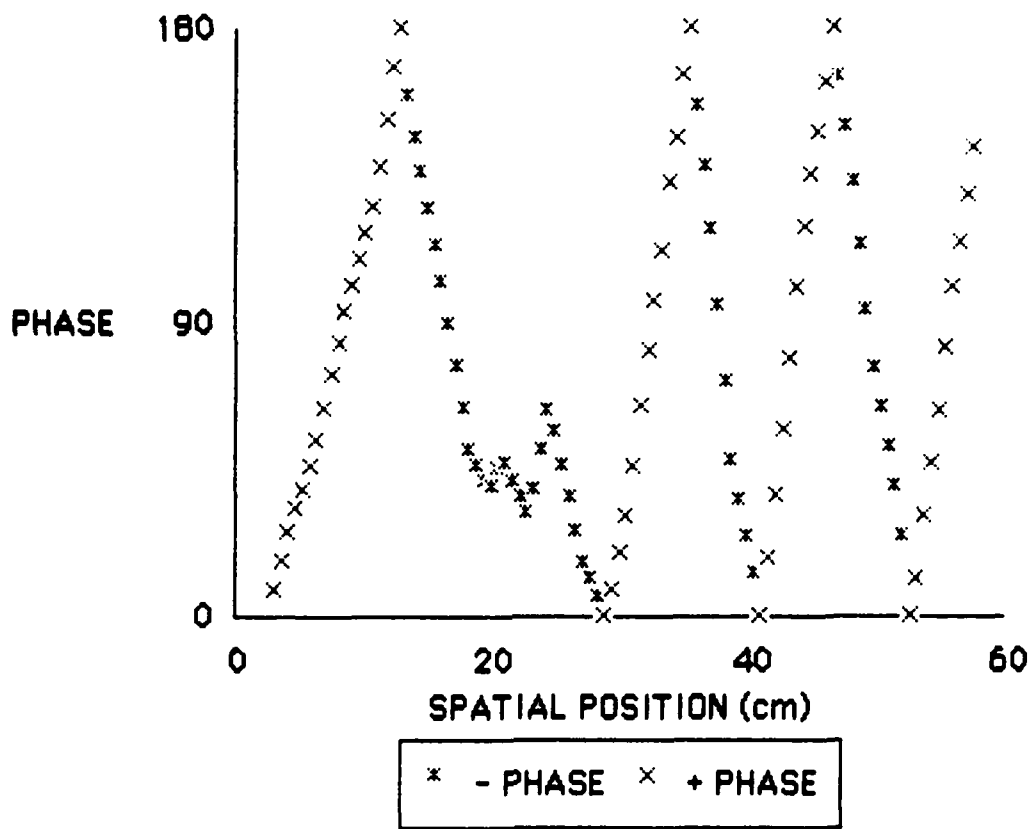**FIGURE 6**
A SAMPLE AMPLITUDE PLOT OF THE OUTPUT OF THE VOLTMETER versus THE
SPATIAL POSITION OF THE HYDROPHONE
THE SAMPLING INCREMENT IS UNIFORM IN CARTESIAN COORDINATE SPACE
THIS REPRESENTS THE AMPLITUDE OF THE PRESSURE FIELD OF THE SCATTERING
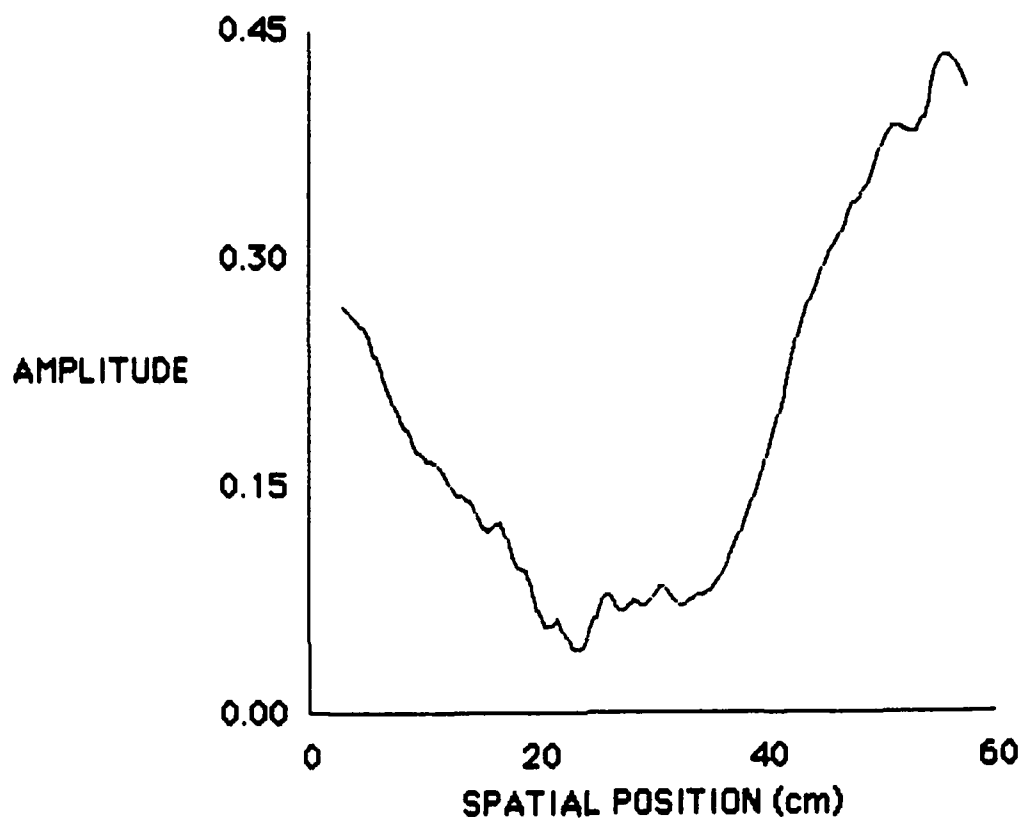FROM ONE INSONIFIED SURFACE SPOT ON SURFACE THREE

35

AS-85-312
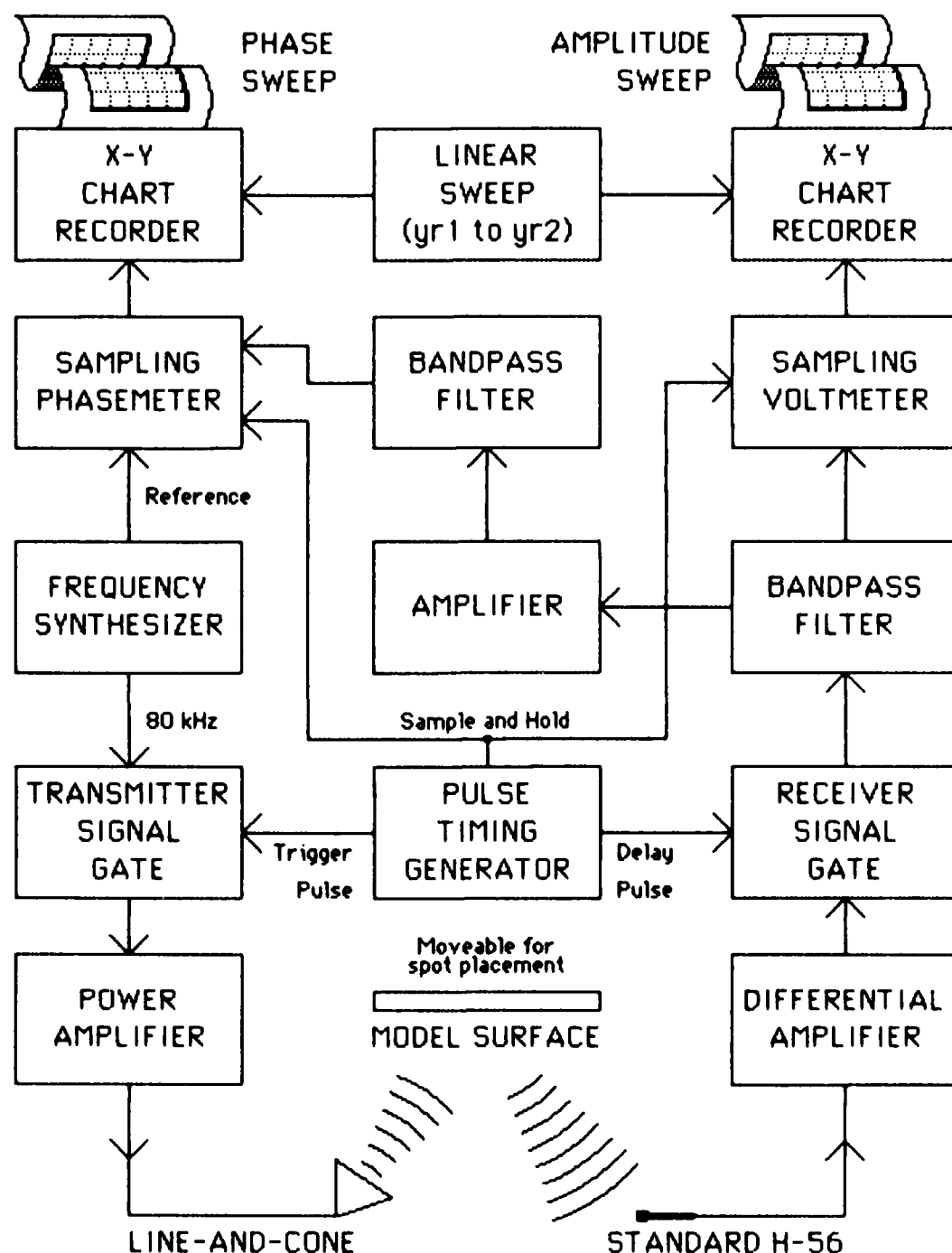
FIGURE 5
DATA ACQUISITION EQUIPMENT FOR EXPERIMENTAL MEASUREMENTS

AS-85-311

from the receiver were amplified and filtered for analysis of phase and amplitude using a pulse phasemeter[34] and voltmeter. The amplitude and phase were recorded using chart recorders in the sweep mode, with the sweep synchronized with the scanning of the field. Figure 5 is a block diagram of the equipment used for data acquisition. The continuous amplitude and phase plots resulting from the above experiments were then digitized for data storage and subsequent processing, examples of which are shown in Figs. 6 and 7. Figure 6 is an amplitude plot of the scattered pressure from one surface spot insonified on surface 3. Figure 7 is the phase plot corresponding to the amplitude plot of Fig. 6.

hydrophone as the omnidirectional receiver. The projector remained fixed at a given angle of incidence upon the surface and the receiver was moved to form an array of pressure measurements. The pressure field was scanned for each insonified area on the model surface to form an ensemble of pressure fields. The projector and receiver coordinates were selected so that shadowing was minimized. When a spot size on the order of a correlation length was insonified neither the projector nor receiver interfered with the other (see Fig. 4).

Due to the finite size of the water tank, a pulsed cw signal was transmitted at a frequency of 80 kHz. The pulse was rectangular with a fixed width and repetition rate. The projector had a -3 dB beamwidth covering a spot of radius 16.5 cm on the surface and an acoustic wavelength of 1.88 cm.

The model surface was located in the farfield of the projector at near-normal incidence producing a -3 dB insonification spot size approximating a circle. A number of spots were insonified leaving an area the size of one spot radius uninsonified at the edge of the surface. The total area insonified was more than half the surface so that the results from the processing could be compared with the physical characteristics of Figs. 2 and 3.

The receiver's active acoustic size was approximately one wavelength in dimension. The receiver was moved by a motorized column in a direction parallel with the model surface. Only the steady state portion of the scattered pulse was sampled for processing. The outputs
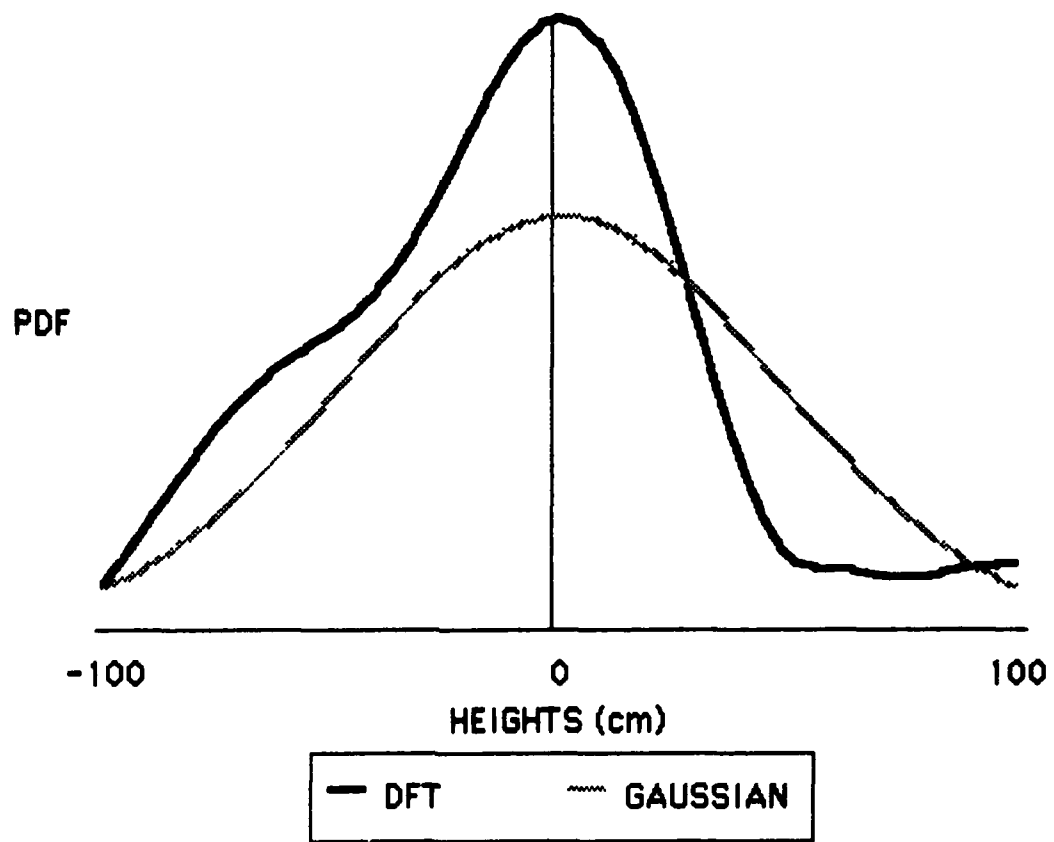
32

FIGURE 11
THE PROBABILITY DENSITY FUNCTION FOR THE THIRD ROUGH
SURFACE VIA THE DISCRETE FOURIER TRANSFORM TECHNIQUE
STANDARD DEVIATION OF THE GAUSSIAN CURVE IS 47.0 cm

46

improved by assuming the characteristic function is zero outside the observation window and computing the FFT with the extended data record thus improving the elementary bandwidth. Although this is cheating, the resolution of the estimate is not improved because of the leakage due to the finite length of the non-zero data. The only improvement is in the view of the finer structure of the PDF.

However, an improvement in the resolution can be seen in the PDF estimate of surface 3 for which the elementary bandwidth is 22 cm. The closest estimate of the rms height (from the DFT) is represented with the Gaussian curve fit of Fig. 9 and is 47.0 cm compared to the true rms height of 0.924 cm. It is obvious that high resolution techniques are necessary for better estimates of the rms height.

2. BLM Technique

Figures 12, 13, and 14 reflect the application of the Bojarsky-Lewis method to the characteristic functions of surfaces 1, 2, and 3. It should be noted that the PDF estimates of Figs. 12 and 13 no longer fit a Gaussian shape due to the appearance of secondary structure. The rms estimates with the least mean square Gaussian fit are therefore deceptive, since it is the central structure of the PDF which should be observed. For a Gaussian curve fit to the central portion, rms height estimates of 71.4 and 82.5 cm are obtained for surfaces 1 and 2. Although the Bojarsky-Lewis method makes use of the discrete Fourier transform, an improvement in resolution is evident, especially in the PDF for surface 3. The rms height for this surface is 8.81 cm, a definite improvement in the estimate. However, it

47

FIGURE 12
THE PROBABILITY DENSITY FUNCTION FOR THE FIRST ROUGH
SURFACE VIA THE BOJARSKY-LEWIS METHOD
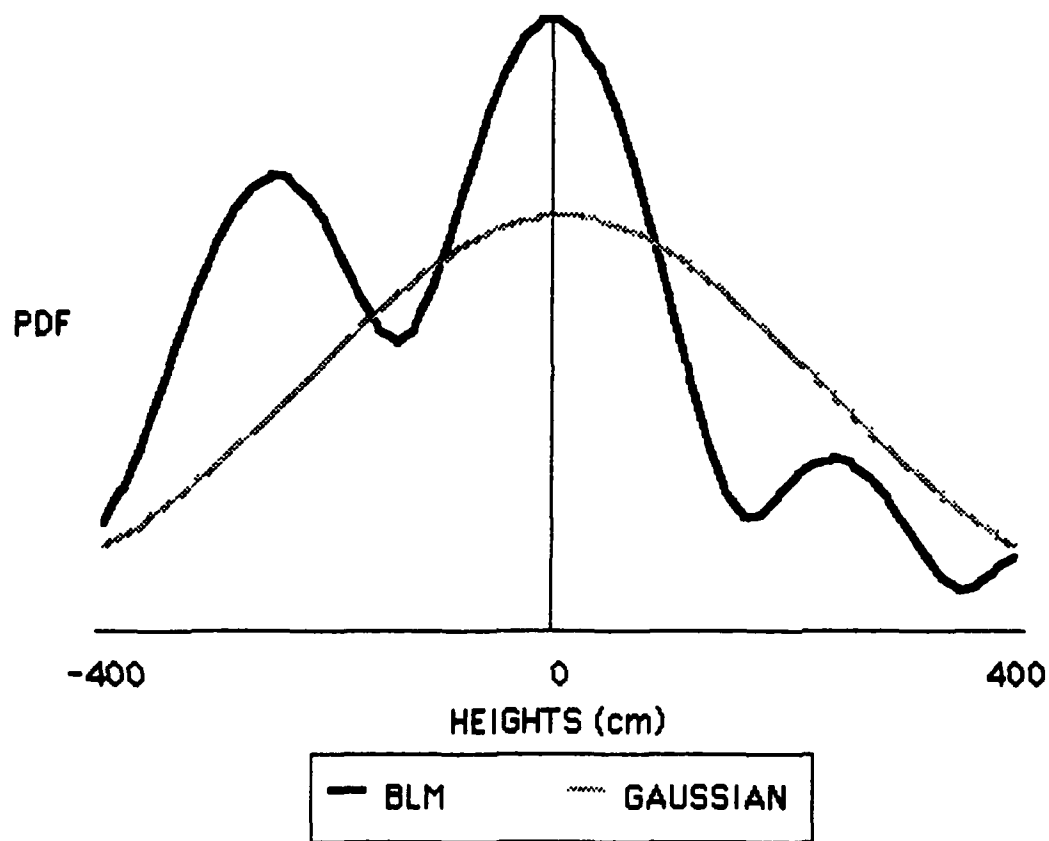STANDARD DEVIATION OF THE GAUSSIAN CURVE IS 224 cm
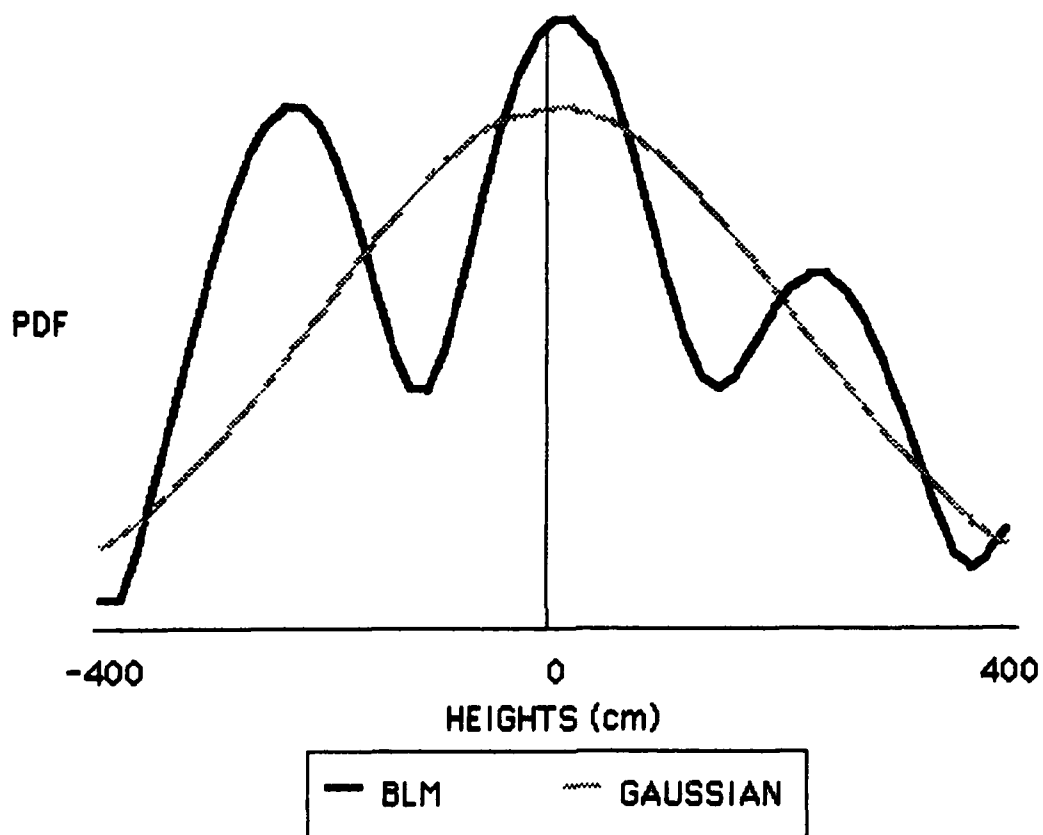
AS-85-318

FIGURE 13
THE PROBABILITY DENSITY FUNCTION FOR THE SECOND ROUGH
SURFACE VIA THE BOJARSKY-LEWIS METHOD
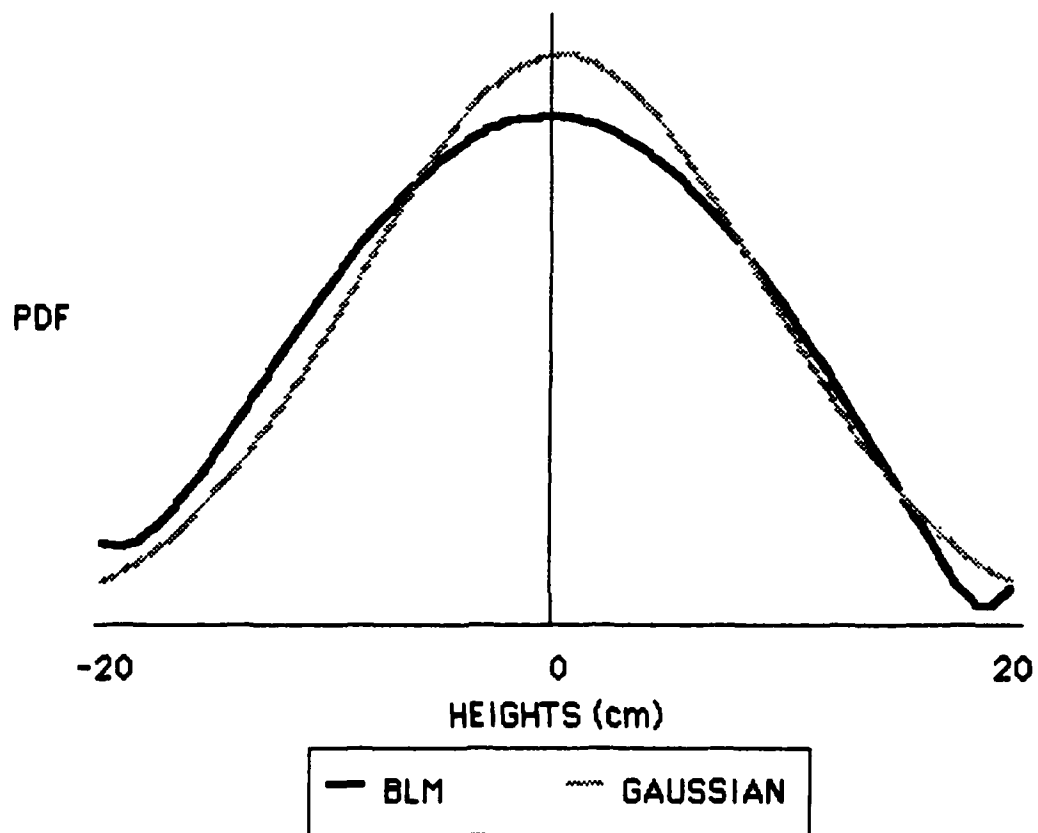STANDARD DEVIATION OF THE GAUSSIAN CURVE IS 208 cm

49

FIGURE 14
THE PROBABILITY DENSITY FUNCTION FOR THE THIRD ROUGH
SURFACE VIA THE BOJARSKY-LEWIS METHOD
STANDARD DEVIATION OF THE GAUSSIAN CURVE IS 8.81 cm

AS-85-320

still does not compare with the true value of 0.924 cm. So it is necessary to use a higher resolution technique.

3. EPM Technique

Figures 15, 16, and 17 show the extended Prony technique applied to the characteristic functions of surfaces 1, 2, and 3. When applied to surfaces 1 and 2, it is noted that the least mean square Gaussian curve does not fit well. When a Gaussian curve is fit to the central portion of the PDF visually, estimates of 32.7 and 41.2 cm are obtained for surfaces 1 and 2. As is expected with the longest data window, the best rms height estimate of 3.2 cm is obtained for the third surface. Fitting the best Gaussian curve to the central portion yields an estimate of 1.4 cm. The steps necessary for further improvement of the estimates are obvious when comparing surfaces 1 and 2 results to surface 3 results. The extension of the length of the data record improves the resolution as expected. Therefore, if the sampling of the characteristic function is extended past the -10 dB points on the image solution, a further improvement in the estimates of the PDF should result. The only other alternative is to use a higher resolution technique for estimation of the PDF.

C. Correlation Estimates

The surface correlation functions were constructed from the normalized spatial correlations of the pressure field of seven different insonification area separations. An example of these spatial correlations for surface 3 is presented in Appendix C. The surface correlation functions

FIGURE 15
THE PROBABILITY DENSITY FUNCTION FOR THE FIRST ROUGH
SURFACE VIA THE EXTENDED PRONY METHOD
STANDARD DEVIATION OF THE GAUSSIAN CURVE IS 62.4 cm

52

FIGURE 16
THE PROBABILITY DENSITY FUNCTION FOR THE SECOND ROUGH
SURFACE VIA THE EXTENDED PRONY METHOD
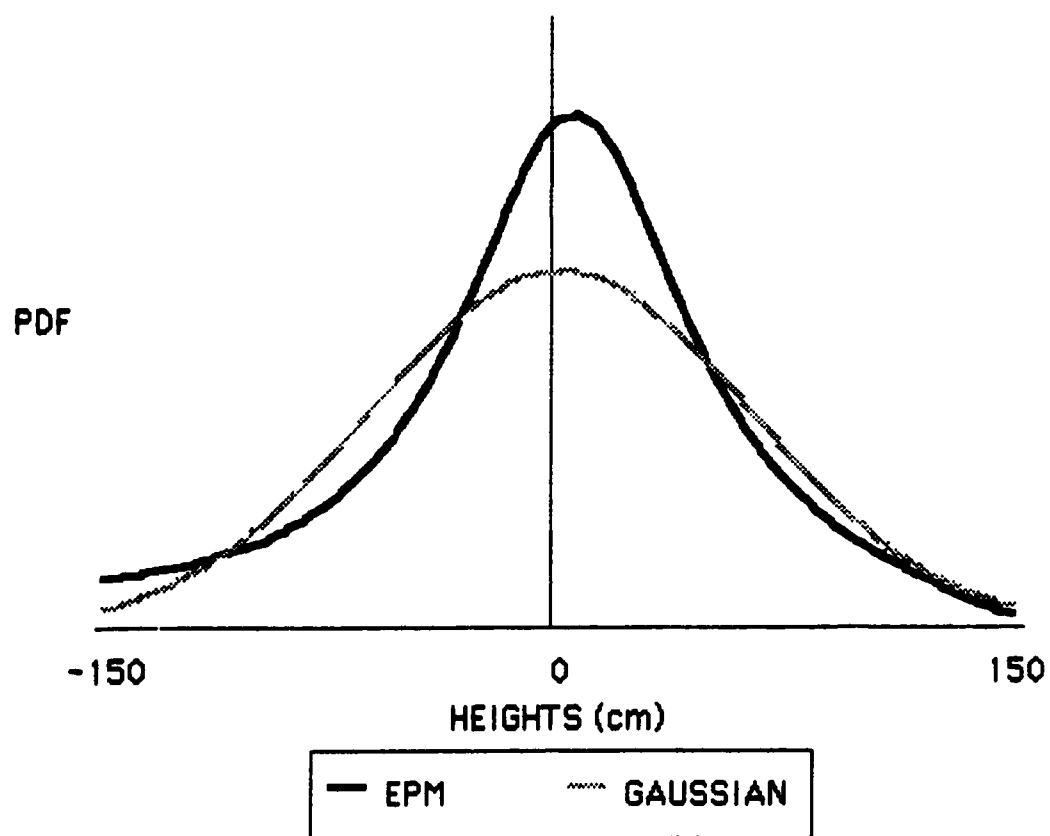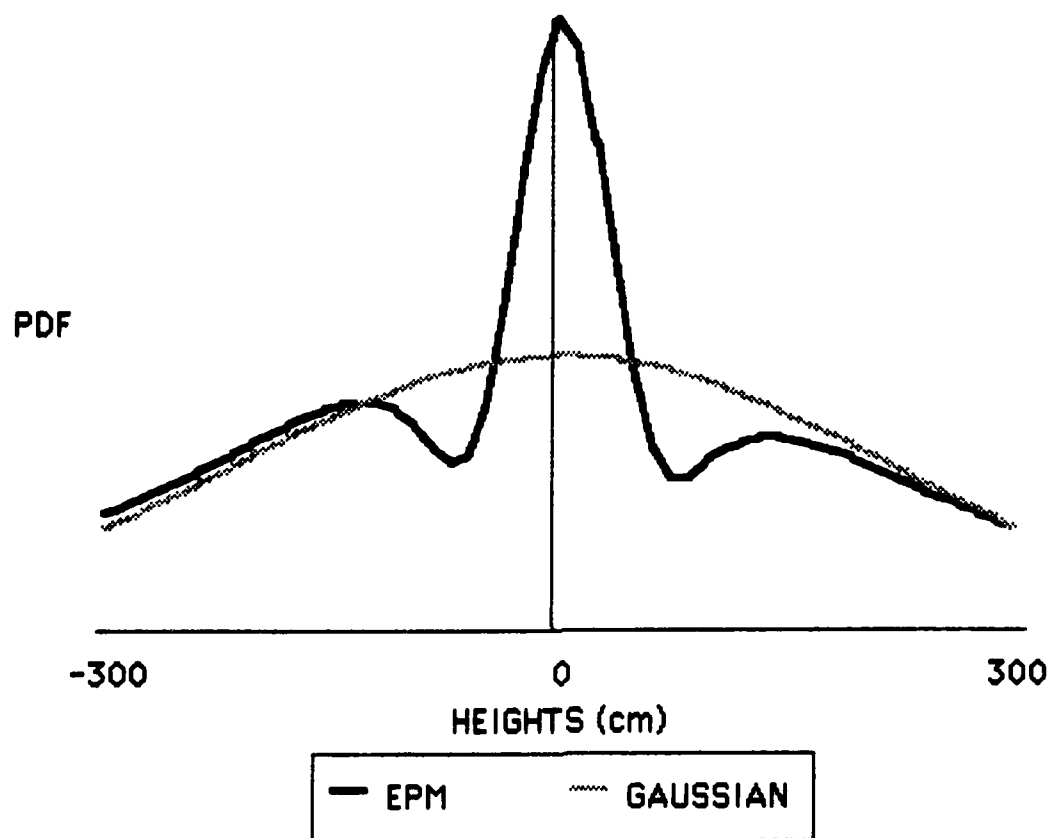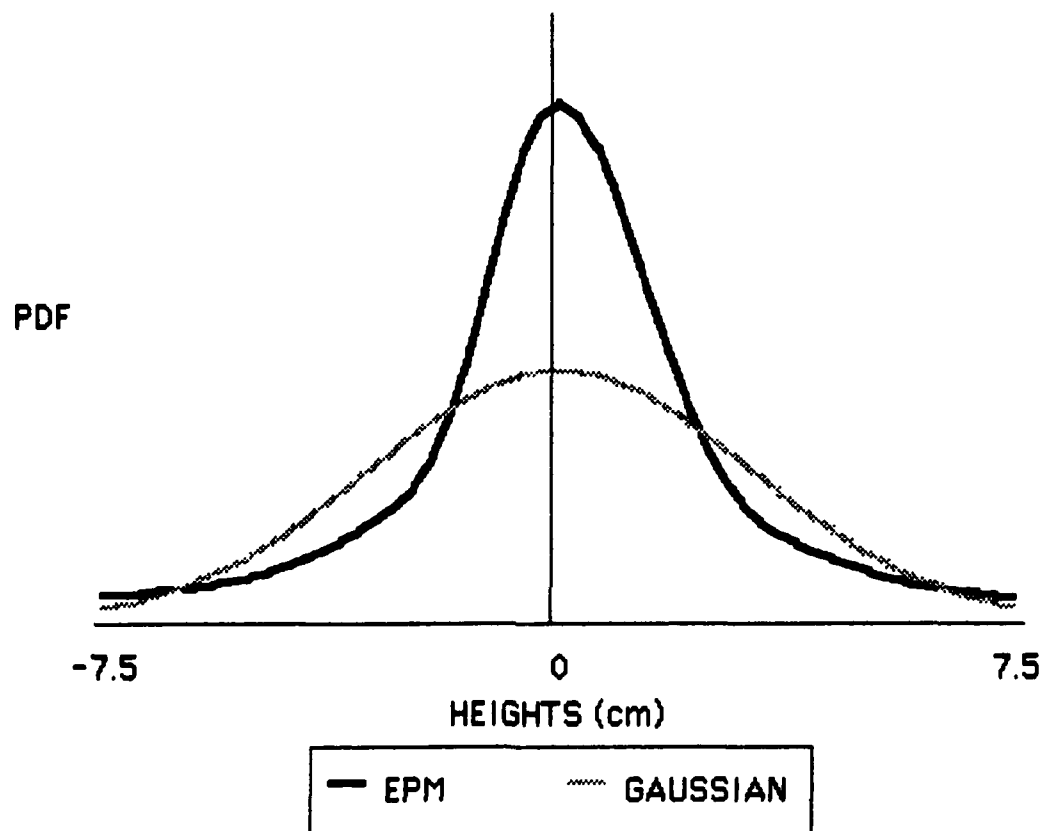STANDARD DEVIATION OF THE GAUSSIAN CURVE IS 215 cm

53

FIGURE 17
THE PROBABILITY DENSITY FUNCTION FOR THE THIRD ROUGH
SURFACE VIA THE EXTENDED PRONY METHOD
STANDARD DEVIATION OF THE GAUSSIAN CURVE IS 3.17 cm

54

of Figs. 18, 19, and 20 are monotonically decreasing, resembling exponential functions. Thus an exponential least squares fit between the data and the analytical function is used to obtain the best fitting function. The correlation lengths calculated represent the e-folding value of the exponential curve. The correlation function fit to surface 1 is reasonably close and yields a correlation length of 7 cm. The least mean square fit for surface 2 does not follow the structure very well, and if an exponential is fit visually a correlation length of 5.5 cm is obtained. The correlation length for surface 3 of 5.2 cm is also reasonable.

The correlation length estimates seem to agree with the physical measurements very well. Many factors have contributed to this agreement. The pressure field is neither oversampled nor undersampled, but sampled sufficiently to yield results unadulterated by the finite extent of the data. Also, the spatial correlations are computed for spots which are incrementally separated a fraction of a correlation length. The variation which does exist is believed to be actually due to the variation of the correlation along different orientations (as in Fig. 3) on the surface; also, the sampling of the pressure field in one dimension allows calculation of the correlation along one axis of the surface.

The results are summarized in Table I. The correlation estimates for surfaces 1, 2, and 3 follow very closely with the actual physical measurements of the correlation lengths.

FIGURE 18
CORRELATION FUNCTION FOR THE FIRST ROUGH SURFACE VIA
THE POWER SPECTRUM OF THE SCATTERED PRESSURE FIELD
THE E-FOLDING VALUE OF THE EXPONENTIAL CURVE IS 7.03 cm

FIGURE 19
CORRELATION FUNCTION FOR THE SECOND ROUGH SURFACE VIA
THE POWER SPECTRUM OF THE SCATTERED PRESSURE FIELD
THE E-FOLDING VALUE OF THE EXPONENTIAL CURVE IS 3.32 cm
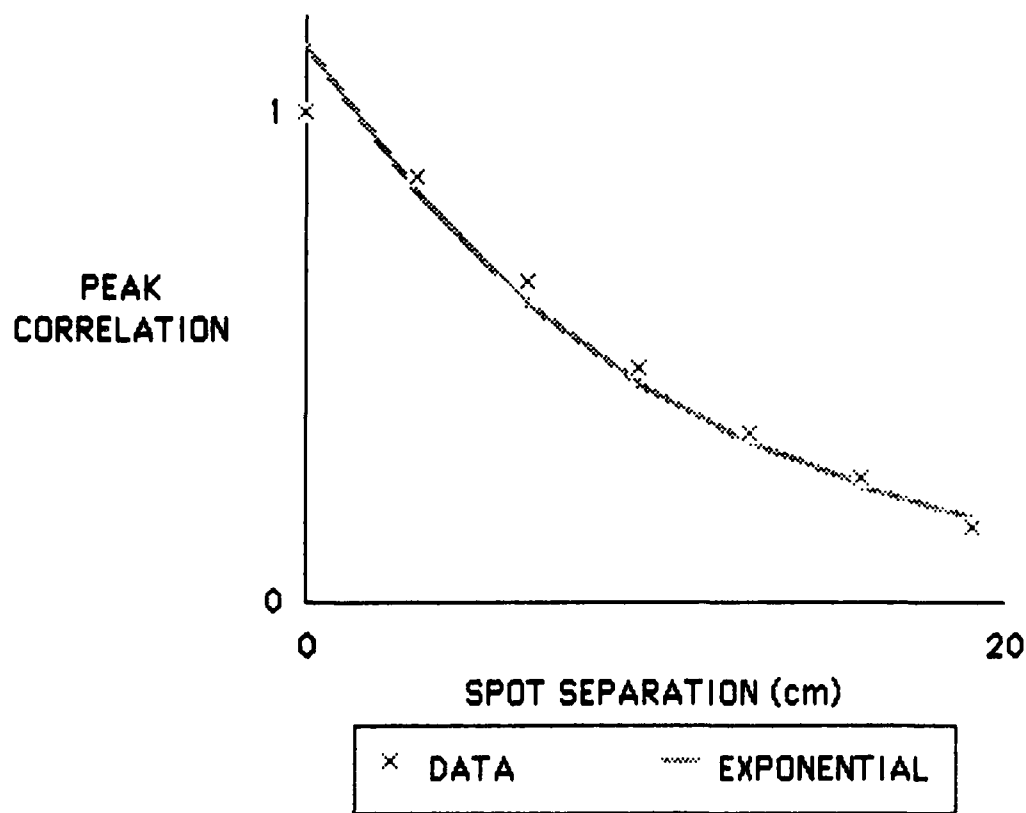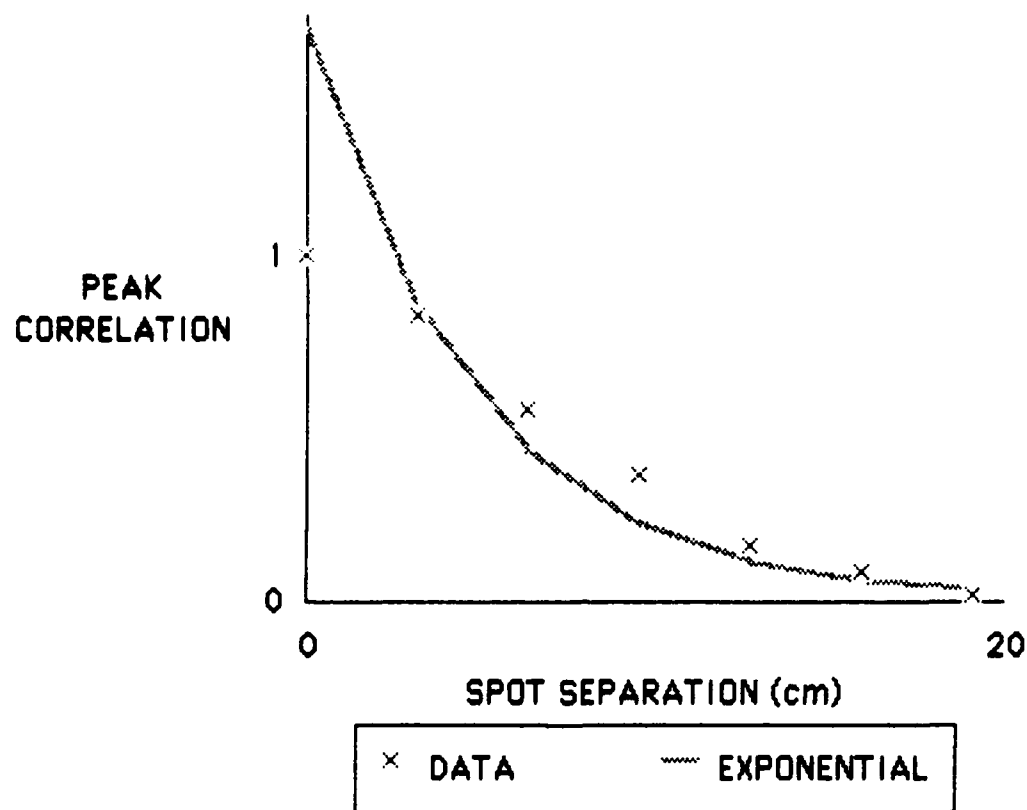
57
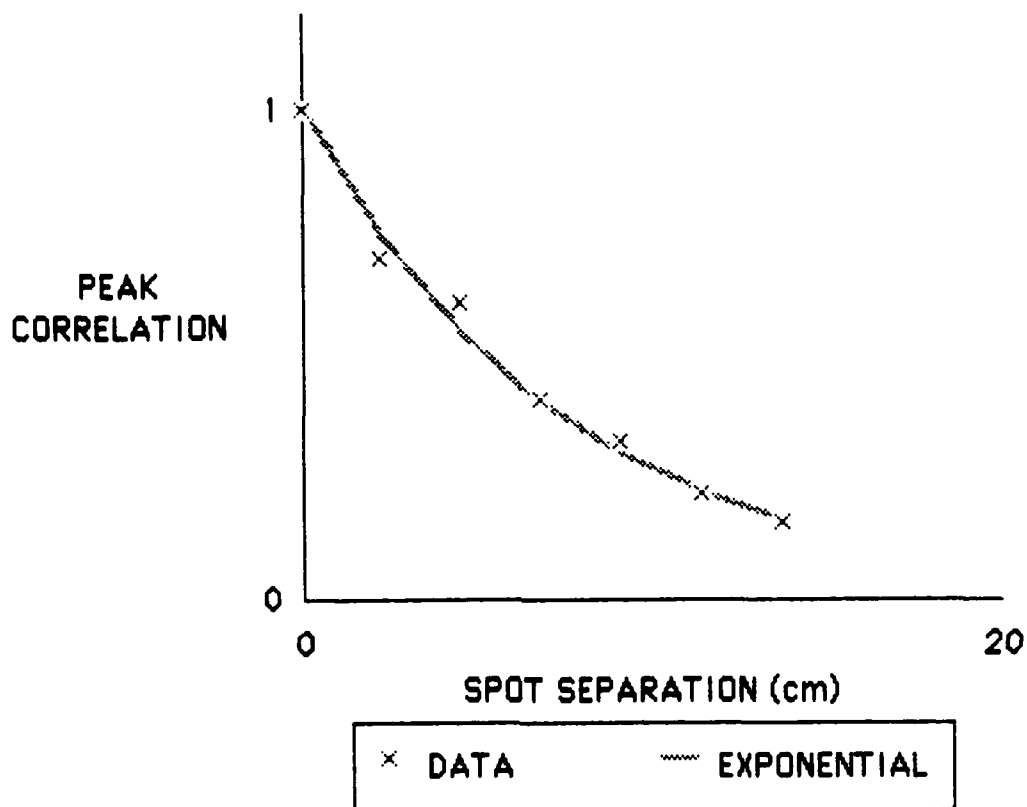
FIGURE 20
CORRELATION FUNCTION FOR THE THIRD ROUGH SURFACE
VIA THE POWER SPECTRUM OF THE SCATTERED PRESSURE FIELD
THE E-FOLDING VALUE OF THE EXPONENTIAL CURVE IS 5.18 cm

58

AS-85-326

VI. CONCLUSIONS

Several techniques have been outlined which have yielded predictions of the probability density function of surface heights and correlation function. The estimates of these statistical characteristics can be obtained directly from measurements of the scattered pressure field from the rough surfaces. Thus the inverse problem has been investigated.

The correlation function estimates agree very well with the measured correlation functions. This is due to two factors: (1) the insonification spots are large compared to the dimensions of the correlation length and (2) the pressure field spot separation and spatial sampling increment are both a fraction of a correlation length in dimension. Therefore, a portion of the surface representative of the surface correlation function has been insonified; and the correlation function estimate has been observed within the resolution bounds necessary to determine correlation length. Thus Clay and Medwin's correlation theory was verified, this time with stationary randomly rough surfaces.

The probability density estimates, although bounded, were not as accurate as the correlation estimates. The estimated rms height values were all exaggerated with the exception of one estimate. From the analysis it is obvious that the experimental constraints have limited the

59

$$\Phi X = W \quad , \qquad\qquad\qquad \text{B.21}$$

where

$$\Phi_{ij} = z_j^{(i-1)} \quad . \qquad\qquad\qquad \text{B.22}$$

$$X = [\, c_1 c_2 \dots c_q \,]^T \quad , \qquad\qquad\qquad \text{B.23}$$

and

$$W = [\, \Omega(0) \dots \Omega(M-1) \,]^T \quad . \qquad\qquad \text{B.24}$$

The form of Φ is a Vandermonde matrix for which a least squares solution is

$$X = [\, \Phi^H \Phi \,]^{-1} \Phi^H W \quad . \qquad\qquad \text{B.25}$$

for H, the complex conjugate transpose.

Combining Eqs. B.13 and B.17 results in

$$\Theta_{j\ell} = \sum_{g=1}^{q} \sum_{h=1}^{q} (C_{gj} {}^{*}C_{g\ell}) \Upsilon_g{}^H \Upsilon_h \qquad \text{B.19}$$

such that Θ will have one eigenvector E_{q+1} which is orthogonal to the q mode vectors, or

$$\Theta E_{q+1} = 0 \qquad \text{B.20}$$

for an eigenvalue of zero.

The procedure for determination of q is to fill the matrix Θ to dimension Q by Q and to calculate the eigenvectors and eigenvalues. If L eigenvalues are equal to zero (or equal to $m\sigma^2$ in the case of data with zero mean noise and variance σ^2), then q=Q-L. The matrix could be recomputed to order q+1 by q+1 and the eigenvectors and eigenvalues regenerated. From Eqs. B.16 and B.20 it is noted that the eigenvector corresponding to a zero eigenvalue is the vector with the coefficients of the difference equation of Eq. B.15. Therefore not only is q achieved but also the $\{a_j\}$.

The polynomial equation of B.7 is rooted to find the $\{z_j\}$ and Eq. B.2 reduces to a set of linear equations which can be written in matrix form,

vector Υ_h starting at the jth ξ step. Recalling Eq. B.4, the mode vectors can be represented with

$$\Upsilon_h = [\, 1 \; z_h^{\,1} \, \dots \, z_h^{\,m}\,]^T \qquad\qquad\qquad \text{B.14}$$

for which there are q vectors.

Now, seeking a solution for the difference equation from Eq. B.10,

$$\sum_{j=0}^{q} a_j \, \Omega(\ell-j) = 0 \,, \; \ell=q, \dots M-1 \quad . \qquad\qquad \text{B.15}$$

A pseudo-inverse solution is achieved for which Eq. B.15 takes on the form

$$\Theta \, A = 0 \quad , \qquad\qquad\qquad\qquad \text{B.16}$$

where Θ is a q+1 by q+1 Hermitian matrix such that

$$\Theta_{j\ell} = D_j^{\,H} D_\ell \qquad\qquad\qquad\qquad \text{B.17}$$

and

$$A = [\, a_0 \; a_1 \, \dots \, a_q\,]^T \qquad\qquad\qquad \text{B.18}$$

rooted to obtain the $\{z_j\}$. Subsequently, the $\{c_j\}$ can be determined by solving the equations of B.2 exactly or by least squares. But a successful application of the EP method depends upon knowledge of the value for q. Many methods have been outlined for the determination of q and the eigenanalysis method outlined by Van Blaricum and Mittra [40] is relatively easy to implement.

We begin with the D_j data vectors

$$D_j = [\ \Omega(q-j) \ \Omega(q-j+1) \ \ldots \ \Omega(q-j+m) \ ]^T \qquad\qquad B.11$$

for m+M-q-1 and T the transpose. These can also be written

$$D_j = \sum_{h=1}^{q} c_h \exp[s_h(q-j)\Delta\zeta] \exp[s_h \ell \Delta\zeta] \ , \ \ell=0, \ldots ,m \qquad B.12$$

or, more simply,

$$D_j = \sum_{h=1}^{q} C_{hj} \Upsilon_h \ , \qquad\qquad B.13$$

where $C_{hj}=c_h\exp[s_h(q-j)\Delta\zeta]$ represents the coefficient for the hth mode

such that $a_0 = -1$ and

$$(z-z_1)(z-z_2)\dots(z-z_q) = 0 \quad . \tag{B.8}$$

A procedure for calculation of the $\{a_j\}$ is now outlined. The first equation in B.2 ($\ell=0$) is multiplied by a_q, the second by a_{q-1}, ..., and the $(q+1)$th by $a_0=-1$ and the sum of the equations is computed. Since each z_j satisfies Eq. B.8 the result is

$$\Omega(q) - a_1\Omega(q-1) - \dots - a_q\Omega(0) = 0 \quad . \tag{B.9}$$

A set of M-q linear equations are thus obtained by using this procedure on the remaining equations of B.2. The resulting equation takes on the form of a familiar set of linear prediction equations,

$$\Omega(\ell) = \sum_{j=1}^{q} a_j \, \Omega(\ell-j) \, , \, \ell = q, \dots, M-1 \quad , \tag{B.10}$$

which can be solved exactly for the $\{a_j\}$, if M=2q, or approximately by a least squares estimation.

After determination of the $\{a_j\}$, the polynomial equation of B.7 is

69

where the α_j is a damping factor. If we also assume that the $\{c_j\}$ are also complex amplitudes,

$$c_j = A_j \exp[i\theta_j] \quad .$$

B.5

then the FT of Eq. B.2 is

$$\omega(\zeta) = \sum_{j=1}^{q} c_j \, 2\alpha_j / [\alpha_j^2 + \{2\pi((\zeta - \zeta_j))\}^2] \quad .$$

B.6

If the $\{z_j\}$ are known, then Eq. B.2 represents a set of M linear equations in q unknowns to be solved for the c_j. For M=q, Eq. B.2 can be solved exactly as Prony[39] had originally intended, and for M<q a linear least squares estimation would obtain the solution, i.e., the EP method. Otherwise the determination of $\{z_j\}$ with known $\{c_j\}$ leads to the solution of a set of nonlinear equations.

Consider the $\{z_j\}$ to be the roots of the polynomial equation

$$\sum_{j=0}^{q} a_j \, z^{(q-j)} = 0$$

B.7

APPENDIX B

DERIVATION OF THE EXTENDED PRONY METHOD

The Prony method consists of expanding the data set known at evenly sampled subintervals with a basis set of complex exponentials, or

$$\Omega(\xi) = \sum_{j=1}^{q} c_j \exp[s_j \xi] \qquad\qquad B.1$$

or, for discrete values of $\xi = \ell \Delta \xi$,

$$\Omega(\ell \xi) = \sum_{j=1}^{q} c_j [z_j]^{\ell} \ , \ \ell = 0,...,M-1 \qquad , \qquad\qquad B.2$$

which looks similar to the DFT expansion. However, unlike the DFT the $\{s_j\}$ are complex in general and non-harmonically related,

$$s_j = \alpha_j + i2\pi\zeta_j \qquad\qquad B.3$$

and

$$z_j = \exp[s_j \Delta \xi] \qquad , \qquad\qquad B.4$$

67

where the $R^{(1)}_{0j}$ are the prolate radial wave functions of the first kind. So Eq. A.13 becomes

$$\omega(\zeta) = \sum_{j=0}^{\infty} \langle v(\zeta), S^{(1)}_{0j}(2\pi\xi_m\zeta_{max}, \zeta/\zeta_{max})\rangle$$
$$\times (2j+1) S^{(1)}_{0j}(2\pi\xi_m\zeta_{max}, \zeta/\zeta_{max})/2 \quad . \qquad\qquad A.17$$

But, from a practical viewpoint, the sum can only be evaluated to a limit

$$\omega(\zeta) = \sum_{j=0}^{J} \langle v(\zeta), S^{(1)}_{0j}(2\pi\xi_m\zeta_{max}, \zeta/\zeta_{max})\rangle/2$$
$$\times (2j+1) \, S^{(1)}_{0j}(2\pi\xi_m\zeta_{max}, \zeta/\zeta_{max}) \quad . \qquad\qquad A.18$$

such that the jth Fourier coefficient of the solution is

$$\langle \omega(\zeta), \eta_j \rangle = \langle v(\zeta), \eta_j \rangle / \lambda_j \quad . \tag{A.12}$$

Therefore, a solution for $\omega(\zeta)$ is

$$\omega(\zeta) = \sum_{j=0}^{\infty} [\langle v(\zeta), \eta_j \rangle / \lambda_j] \, \eta_j(\zeta) \tag{A.13}$$

for $-\zeta_{max} < \zeta < +\zeta_{max}$ and the series is convergent in the mean square sense.

The η_j are related to the prolate angular wave functions of the first kind, $S^{(1)}_{0j}$, through

$$\eta_j(\zeta) = \sqrt{\lambda_j} \, S^{(1)}_{0j}(2\pi\xi_m\zeta_{max}, \zeta/\zeta_{max}) / \mu_j \quad . \tag{A.14}$$

where

$$\mu_j = \sqrt{[2/(2j+1)]} \tag{A.15}$$

and

$$\lambda_j = 4 \, \xi_m \, \zeta_{max} \, [R^{(1)}_{0j}(2\pi\xi_m\zeta_{max}, 1)]^2 \tag{A.16}$$

$$\langle a, b \rangle = \int_{-\zeta max}^{+\zeta max} a(\zeta)\, b(\zeta)\, d\zeta \quad . \tag{A.8}$$

Although not explicitly indicated, the ϕ_j and λ_j also depend upon the product $2\pi \zeta_m \zeta_{max}$.

Slepian and Pollack[38] describe a set of functions

$$\{\eta_j(\zeta)\} = \{\sqrt{[\lambda_j]}\, \phi_j(\zeta)\} \tag{A.9}$$

which are orthonormal in the space of square integrable functions over the ζL range. Multiplying both sides of Eq. A.4 by η_j and integrating over $-\zeta_{max}$ to $+\zeta_{max}$ gives

$$\langle v(\zeta), \eta_j(\zeta) \rangle = \left\langle \int_{-\zeta max}^{+\zeta max} \omega(x)\, sinc(\zeta - x)\, dx\, , \eta_j(\zeta) \right\rangle \quad . \tag{A.10}$$

The symmetric nature of the kernel and Eq. A.9 allows Eq. A.10 to be rewritten as

$$\langle v(\zeta), \eta_j(\zeta) \rangle = \lambda_j \langle \omega(\zeta), \eta_j(\zeta) \rangle \tag{A.11}$$

ζ_{max}.

$$v(\zeta) = \int_{-\zeta_{max}}^{+\zeta_{max}} \omega(x)\, \text{sinc}(\zeta - x)\, dx \quad . \qquad\qquad A.4$$

The kernel of this integral equation therefore has a countably infinite set of eigenfunctions

$$\{\phi_j(\zeta)\}, \; j = 0, 1, \ldots \quad , \qquad\qquad A.5$$

corresponding to positive eigenvalues

$$\lambda_0 > \lambda_1 > \lambda_2 > \ldots > 0 \qquad\qquad A.6$$

such that the set $\{\phi_j(\zeta)\}$ is complete in the space of square integrable functions over the ζL range. Also the ϕ_j are orthogonal over the ζL range,

$$\langle \phi_j, \phi_\ell \rangle = 0, \; j \neq \ell$$
$$= 1, \; j = \ell \qquad\qquad A.7$$

for $j, \ell = 0, 1, \ldots,$ and where the inner product is defined with

APPENDIX A

DERIVATION OF THE BOJARSKY-LEWIS METHOD

The Bojarsky-Lewis method is developed for ξL functions. Since the data are finite in extent, it is assumed that a rectangular window $U(\xi)$ is chosen such that

$$U(\xi) = 1 \ , \ \xi_{min} \leq \xi \leq \xi_{max}$$
$$= 0 \ , \text{ otherwise} \qquad\qquad\qquad A.1$$

and, when applied to the characteristic function, yields

$$V(\xi) = U(\xi)\,\Omega(\xi) \quad . \qquad\qquad\qquad A.2$$

Assuming that Ω is known over the ξL range and that $V(\xi)$ has an inverse FT, Eq. A.2 when inverse transformed and the convolution theorum invoked becomes

$$v(\zeta) = \int_{-\infty}^{+\infty} \omega(\kappa)\,\text{sinc}(\zeta-\kappa)\,d\kappa \qquad\qquad A.3$$

for v, the inverse FT of V.

For a real surface ζ is bounded and ∞ in Eq. A.3 is replaced with

reflection).   Also Stanton[34] has successfully implemented a pressure amplitude analysis in an inverse type problem. Powell[37] used this method in an analysis of the author's scattered pressure data.

In general, the objectives of the inverse problem in estimating the statistical parameters of a randomly rough scattering surface were accomplished with some limited success.

resolution. Perhaps the most critical constraint is the imposition of a very small beamwidth source to insonify small spots on the surfaces. This results in a scattered pressure field which is very limited in angular extent resulting in a very small observation window. With the additional constraint of a single frequency of incident pressure, this limits the observation window of the wave number space of the characteristic function of surface heights. An additional limitation to the resolution is introduced by the choice of near-normal incidence to minimize shadowing and neglecting surface slopes and multiple scattering.

Various improvements can be made to increase the resolution of the experiment and as a result the accuracy of the PDF estimates. The first improvement is of course to use the current acoustic model and simply increase the observation window. But this would mean using a larger beamwidth source, thus requiring a larger model rough surface so that a representative number of spots could be insonified. Secondly, higher resolution spectrum analysis techniques could be used, for example, maximum likelihood, maximum entropy, etc.

A third alternative is to use a different acoustic scattering model. This could be done by modifying the present theory to account for broadband incident energy, shadowing, slopes, or multiple scattering. The result, though, would be most certainly non-trivial. Clay and Medwin[19] were successful in applying the present theory for finding the PDF when they used various frequencies of incident pressure to sample the surface wave number space (instead of varying the angles of incidence and

APPENDIX C

SPATIAL CORRELATION FUNCTION

The spatial correlation function of the pressure field contains information which will allow the inference of the correlation function of the scattering surface. In order to study the form of the spatial correlation function suggested by Clay and Medwin, the spatial pressure field was recorded for the insonification of different areas on the model rough surface. The pressure field was then spatially correlated by computing the correlation between the pressure fields of spots which have been separated a given distance (for all possible combinations of spots being separated that distance). Figure C-1 represents the total number of spots which were insonified on surface 3. All possible combinations of the various spot separations are also listed by the number of separated spot pairs. Figures C-2 through C-8 represent the spatial correlations of the pressure fields from each spot separation. It should be noted that for greater separations the maximum of the correlation function decreases and is shifted from the origin an amount proportional to the spot separation.
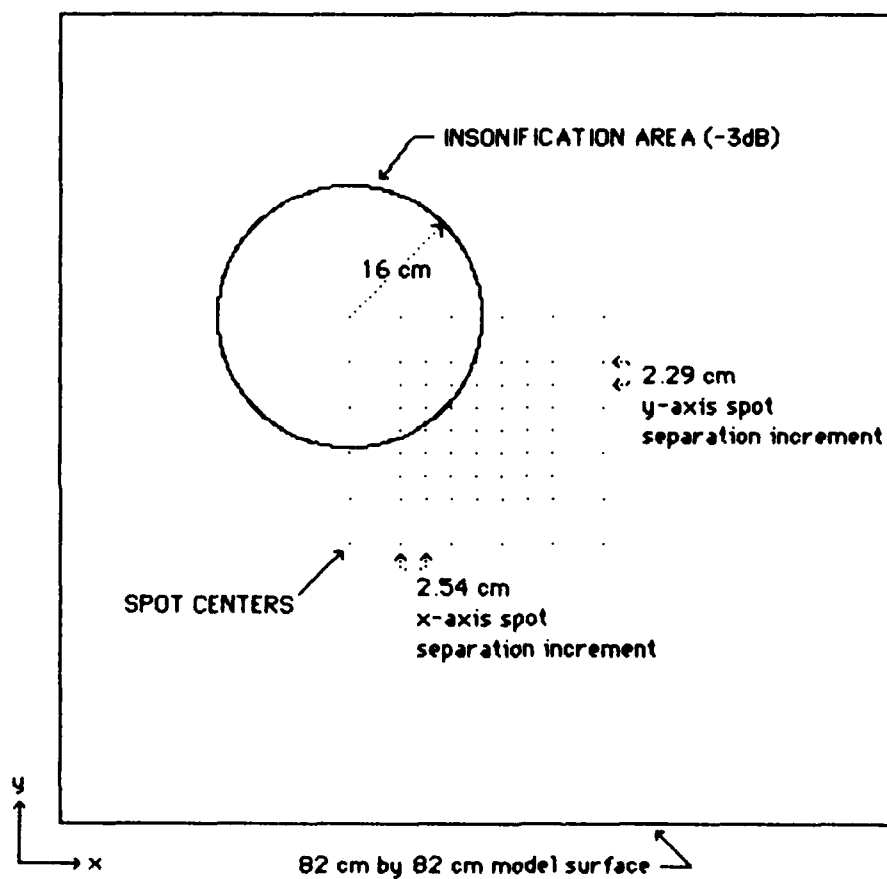
Spot
Separation (cm)

Spot Separation (cm)	0.0	2.29	4.58	6.87	9.16	11.5	13.7
# Spot Pairs	69	42	53	36	37	22	21

FIGURE C-1
LOCATION OF THE 69 SURFACE INSONIFICATION AREAS
(-3 dB SPOT AREA) ON THE THIRD ROUGH SURFACE

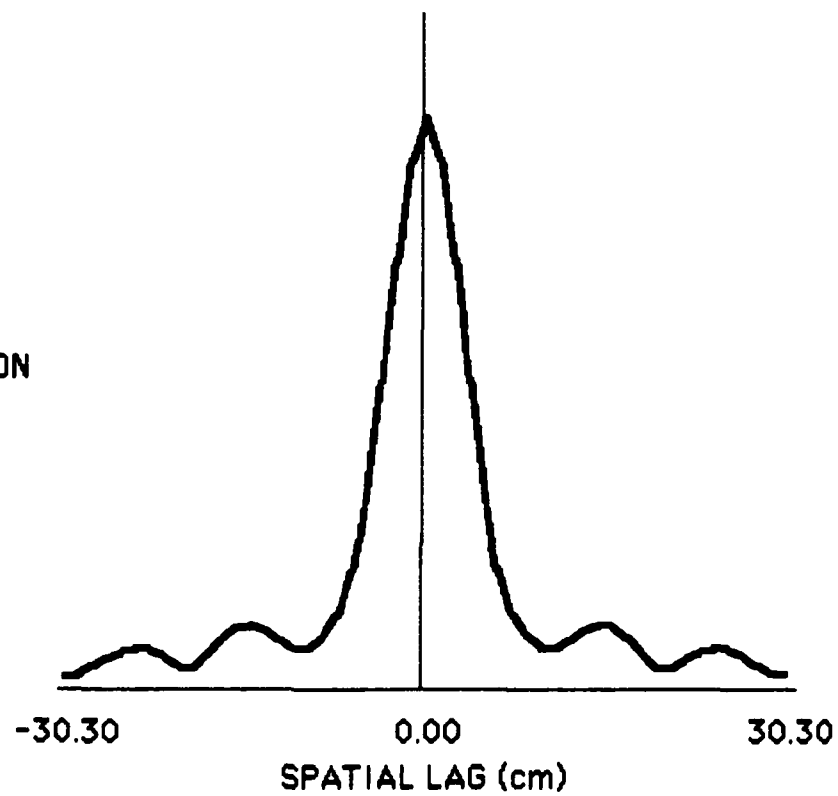75

SPATIAL
CORRELATION

SPATIAL LAG (cm)

FIGURE C-2
SPATIAL CORRELATION FUNCTION OF THE SCATTERED PRESSURE
FIELD FOR SPOTS SEPARATED BY 0 cm
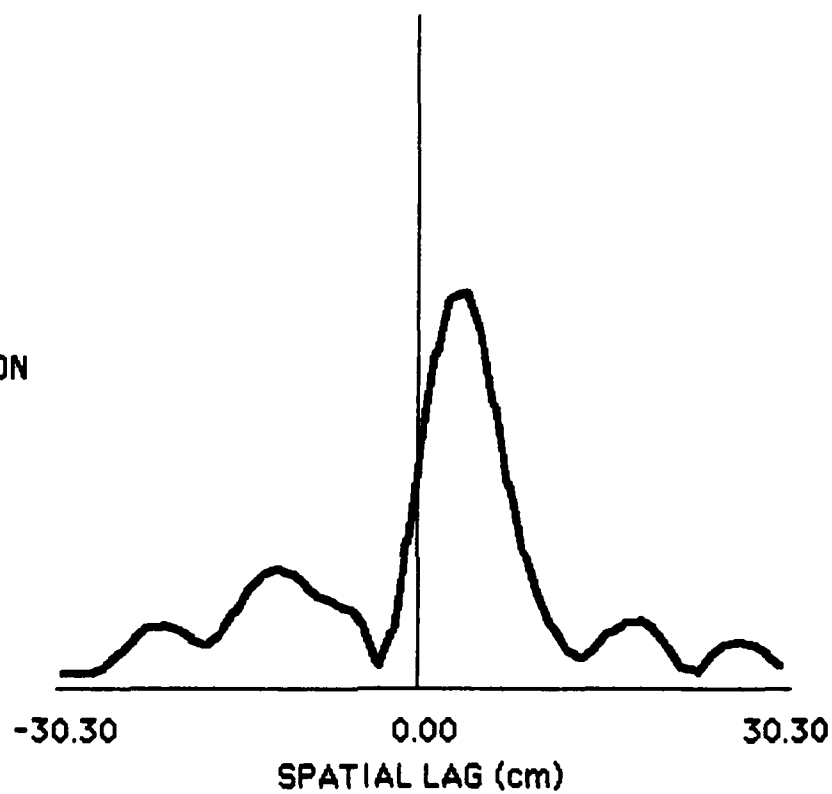THE MAXIMUM CORRELATION VALUE IS 1 AT A SPATIAL LAG OF 0 cm

76

AS-85-328

FIGURE C-3
SPATIAL CORRELATION OF THE SCATTERED PRESSURE
FIELD FOR SPOTS SEPARATED BY 2.29 cm
THE MAXIMUM CORRELATION VALUE IS 0.695 AT A SPATIAL LAG OF 3.64 cm

77

FIGURE C-4
SPATIAL CORRELATION FUNCTION OF THE SCATTERED PRESSURE
FIELD FOR SPOTS SEPARATED BY 4.58 cm
THE MAXIMUM CORRELATION VALUE IS 0.604 AT A SPATIAL LAG OF 6.06 cm

AS-85-330

SPATIAL
CORRELATION

-30.30   0.00   30.30
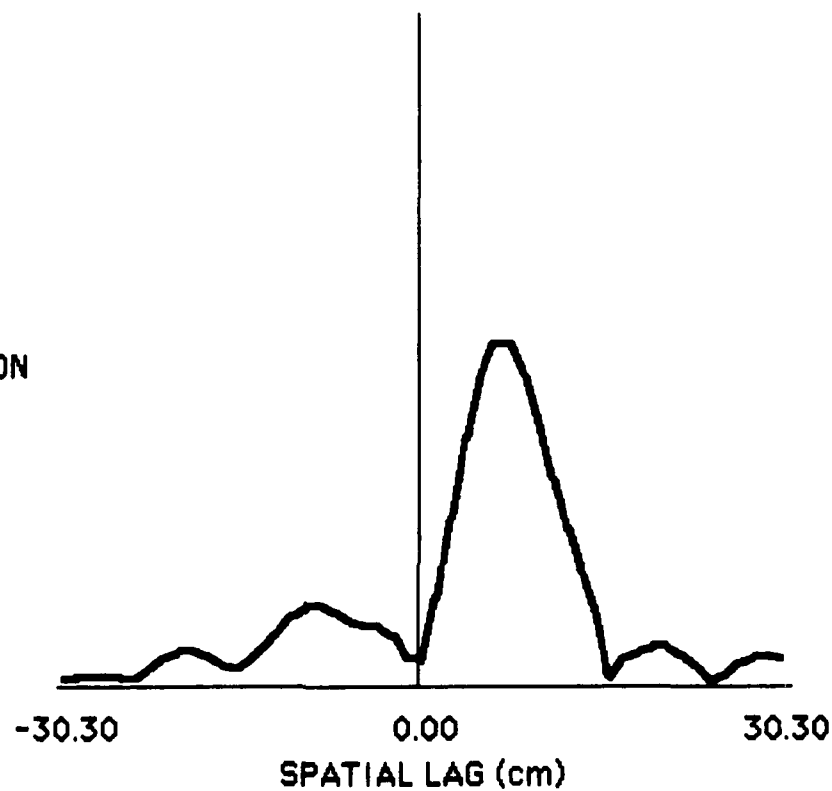SPATIAL LAG (cm)

FIGURE C-5
SPATIAL CORRELATION FUNCTION OF THE SCATTERED PRESSURE
FIELD FOR SPOTS SEPARATED BY 6.87 cm
THE MAXIMUM CORRELATION VALUE IS 0.406 AT A SPATIAL LAG OF 9.7 cm

79

AS-85-331

SPATIAL
CORRELATION

-30.30   0.00   30.30

SPATIAL LAG (cm)

FIGURE C-6
SPATIAL CORRELATION FUNCTION OF THE SCATTERED PRESSURE
FIELD FOR SPOTS SEPARATED BY 9.16 cm
THE MAXIMUM CORRELATION VALUE IS 0.324 AT A SPATIAL LAG OF 14.5 cm

AS-85-332

FIGURE C-7
SPATIAL CORRELATION FUNCTION OF THE SCATTERED PRESSURE
FIELD FOR SPOTS SEPARATED BY 11.5 cm
THE MAXIMUM CORRELATION VALUE IS 0.214 AT A SPATIAL LAG OF 18.2 cm

81

SPATIAL
CORRELATION

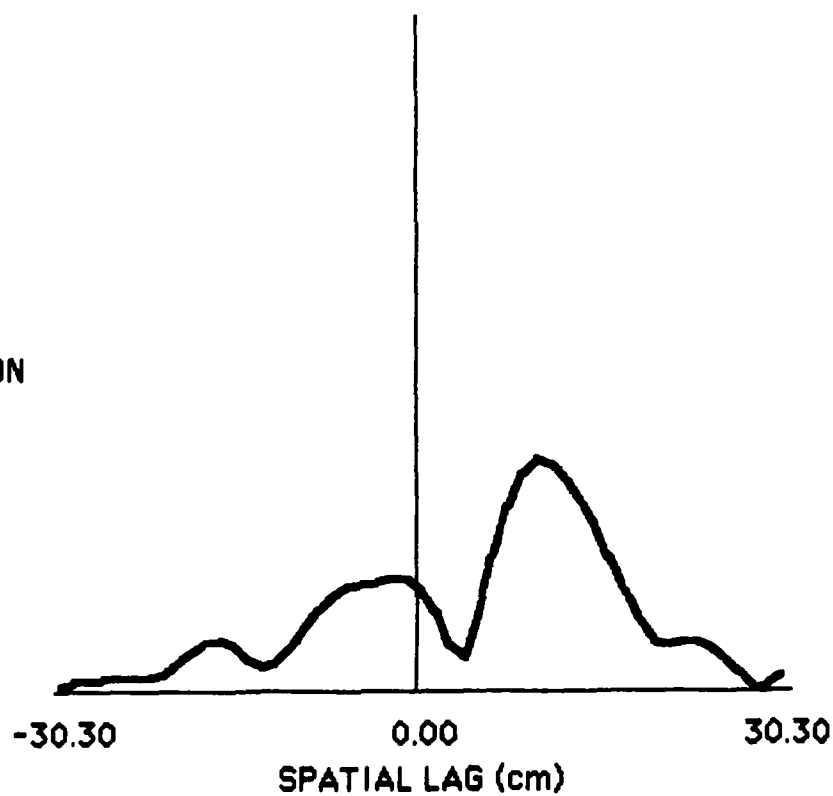-30.30   0.00   30.30
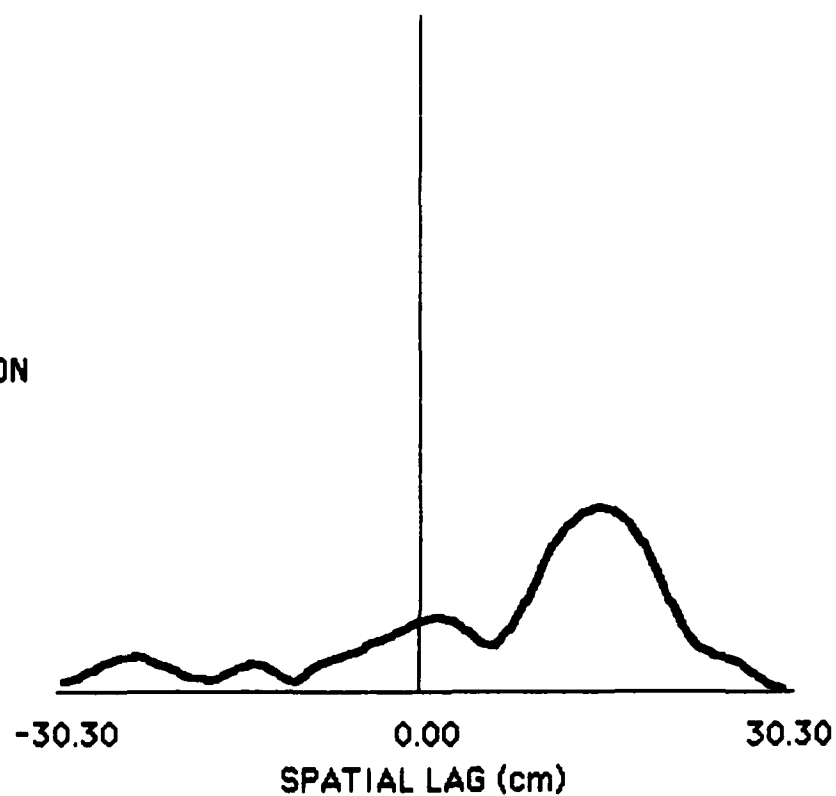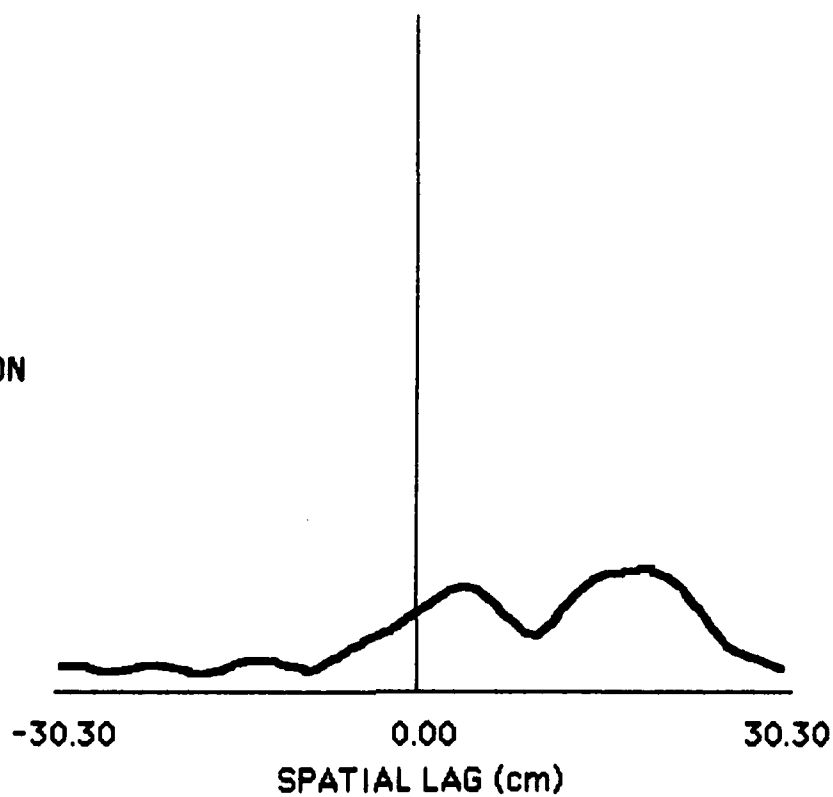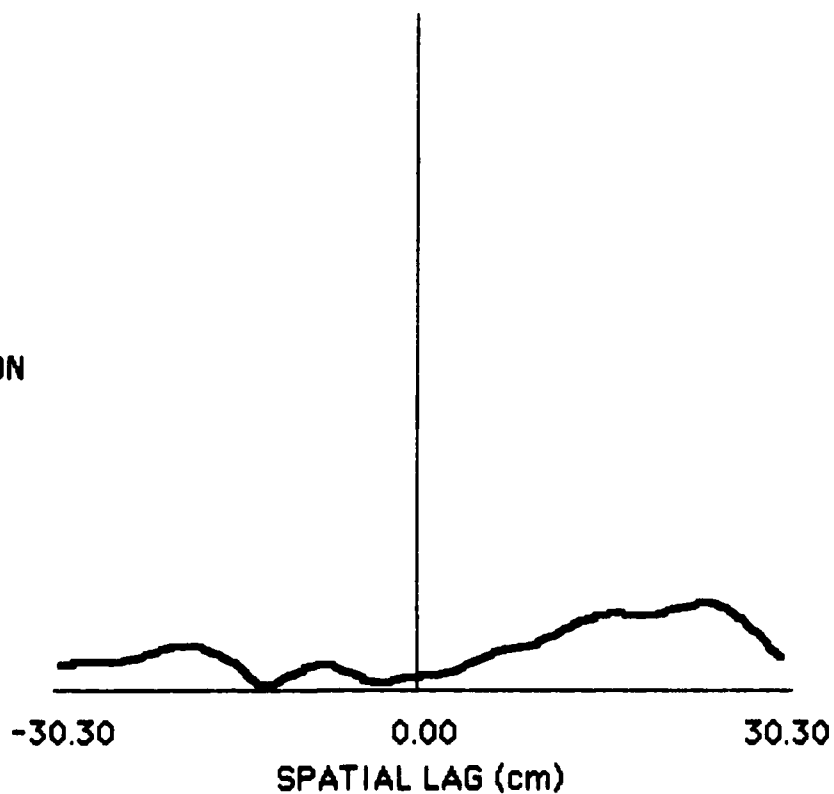
SPATIAL LAG (cm)

FIGURE C-8
SPATIAL CORRELATION FUNCTION OF THE SCATTERED PRESSURE
FIELD FOR SPOTS SEPARATED BY 13.7 cm
THE MAXIMUM CORRELATION VALUE IS 0.155 AT A SPATIAL LAG OF 24.2 cm

82

REFERENCES

1. Z. S. Agranovich and V. A. Marchenko, The Inverse Problem of Scattering Theory (Gordon and Breach, New York, 1963).

2. K. Chadan and P. C. Sabatier, Inverse Problems in Quantum Scattering Theory (Springer-Verlag, Heidelberg, Berlin, 1977).

3. N. Bleistein and J. K. Cohen, "Nonuniqueness in the Inverse Source Problem in Acoustics and Electromagnetics," J. Math. Phys. 18, 194-201 (1977).

4. Special Issue on Inverse Methods in Electromagnetics, IEEE Trans. Antennas Propag. AP-29, Part I, No. 2 (1981).

5. J. W. Strutt (Lord Rayleigh), The Theory of Sound (The MacMillan Company, London, England, 1926), Vol. II, Sec. 272.

6. L. Fortuin, "Survey of Literature on Reflection and Scattering of Sound Waves at the Sea Surface," J. Acoust. Soc. Am. 47, 1204-1228 (1970).

7. C. W. Horton, Sr., "A Review of Reverberation, Scattering and Echo Structure," J. Acoust. Soc. Am. 51, 1049-1061 (1972).

8. D. Middleton, "A Statistical Theory of Reverberation and Similar First-order Scattered Fields: Parts I and II," IEEE Trans. Inf. Theory IT-13, 372-414 (1967).

9. C. Eckart, "The Scattering of Sound from the Sea Surface," J. Acoust. Soc. Am. 25, 566-570 (1953).

10. P. Beckmann and A. Spizzichino, The Scattering of Electromagnetic Waves from Rough Surfaces (The MacMillan Company, New York, 1963).

11. C. W. Horton, Sr., and T. G. Muir, "Theoretical Studies on the Scattering of Acoustic Waves from a Rough Surface," J. Acoust. Soc. Am. 41, 627-634 (1967).

12. C. W. Horton, Sr., S. K. Mitchell, and G. R. Barnard, "Model Studies on the Scattering of Acoustic Waves from a Rough Surface," J. Acoust. Soc. Am. 41, 635-643 (1967).

13. P. J. Welton, H. G. Frey, and P. Moore, "Experimental Measurements of the Scattering of Acoustic Waves from a Rough Surface," J. Acoust. Soc. Am. 52, 1553-1563 (1972).

14. M. L. Boyd and R. L. Deavenport, "Forward and Specular Scattering from a Rough Surface: Theory and Experiment," J. Acoust. Soc. Am. 53, 791-801 (1973).

15. S. K. Mitchell, "Underwater Sound Scattering from an Irregular Surface," thesis presented to Department of Physics, The University of Texas at Austin, Austin, Texas (1966).

16. D. R. Melton, "Specular Scattering of Acoustic Waves from a Rough Surface in the Fraunhofer and Fresnel Approximation," Ph.D. dissertation presented to the Department of Physics, The University of Texas at Austin, Austin, Texas (1969).

17. P. J. Welton, "A Theoretical and Experimental Investigation of the Scattering of Acoustic Waves by Randomly Rough Surfaces," Ph.D. dissertation presented to the Department of Physics, The University of Texas at Austin, Austin, Texas (1975).

18. C. S. Clay and H. Medwin, "Dependence of Spatial and Temporal Correlation of Forward Scattered Underwater Sound on the Surface Statistics, I. Theory, and II. Experiment," J. Acoust. Soc. Am. 47, 1412-1429 (1970).

19. C. S. Clay, H. Medwin, and W. M. Wright, "Specularly Scattered Sound and the Probability Density Function of a Rough Surface," J. Acoust. Soc. Am. 53, 1677-1682 (1973).

20. J. M. Proud, Jr., R. T. Beyer, and P. Tamarkin, "Reflection of Sound from Randomly Rough Surfaces," J. Appl. Phys. 31, 543-553 (1960).

21. B. E. Parkins, "Scattering from the Time-Varying Surface of the Ocean," J. Acoust. Soc. Am. 42, 1262-1267 (1967).

22. C. W. Horton, Sr., W. B. Hempkins, and A. A. J. Hoffman, "A Statistical Analysis of Some Aeromagnetic Maps from the Northwestern Canadian Shield," Geophysics 29, 582-601 (1964).

23. P. M. Morse and H. Feshbach, Methods of Theoretical Physics (McGraw-Hill Book Co., Inc., New York, 1953), Part 1, 806-807.

24. A. Sommerfeld, Optics (Academic Press, New York, 1954), 199-201.

25. L. M. Spetner, "A Statistical Model for Forward Scattering of Waves off a Rough Surface," IEEE Trans. Antennas Propag. AP-6, 88 (1958).

26. A. Papoulis, The Fourier Integral and its Applications (McGraw-Hill Book Co., Inc., New York, 1961).

27. E. O. Brigham, The Fast Fourier Transform (Prentice-Hall, Inc., Englewood Cliffs, 1974).

28. F. J. Harris, "On the Use of Windows for Harmonic Analysis with the Discrete Fourier Transform," Proc. IEEE 66, 51-83 (1978).

29. W. L. Perry, "On the Bojarsky-Lewis Inverse Scattering Method," IEEE Trans. Antennas Propag. AP-22, 826-828 (1974).

30. S. M. Kay and S. L. Marple, Jr., "Spectrum Analysis--A Modern Perspective," Proc. IEEE 69, 1380-1419 (1981).

31. A. V. Oppenheim and R. W. Shafer, <u>Digital Signal Processing</u> (Prentice-Hall, Inc., Englewood Cliffs, 1975).

32. P. J. Welton, K. E. Hawker, Jr., and H. G. Frey, "Experimental Shadowing Measurements of Randomly Rough Surfaces," J. Acoust. Soc. Am. <u>54</u>, 446-450 (1973).

33. D. L. Baird and C. M. McKinney, "Investigation of the Line-and-Cone Underwater Sound Transducer," J. Acoust. Soc. Am. <u>34</u>, 1576-1581 (1962).

34. T. K. Stanton, "Sonar Estimates of Sea Floor Microroughness," J. Acoust. Soc. Am. <u>75</u>, 809-818 (1984).

35. R. S. Bailey, "A Sampling Phasemeter Design for Pulsed Continuous Wave Signals," Applied Research Laboratories Technical Report No. 85-5 (ARL-TR-85-5), Applied Research Laboratories, The University of Texas at Austin (1985).

36. B. J. Patz and A. L. Van Buren, "A FORTRAN Computer Program for Calculating the Prolate Spheroidal Angular Functions of the First Kind," NRL Memorandum Report 4414, Naval Research Laboratory, Washington D.C. (1981).

37. J. Powell, "Envelope Analysis of Inverse Scattering Data," in "The Department of Defense Science and Engineering Apprenticeship Program for High School Students," Applied Research Laboratories Technical Report No. 84-28 (ARL-TR-84-28), Applied Research Laboratories, The University of Texas at Austin (1984), pp. 75-92.

38. D. Slepian and H. O. Pollak, "Prolate Spheroidal Wave Functions, Fourier Analysis and Uncertainty--I," Bell Syst. Tech. J. <u>40</u>, 43-64 (1961).

39. R. Prony, "Essai Experimental et Analytique...," Paris J. l'Ecole Polytechnique <u>1</u>, 24-76 (1795).

40. M. L. Van Blaricum and R. Mittra, "Problems and Solutions Associated with Prony's Method for Processing Transient Data," IEEE Trans. Antennas Propag. <u>AP-26</u> 174-182 (1978).
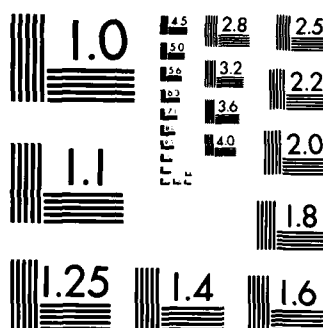
MICROCOPY RESOLUTION TEST CHART

NATIONAL BUREAU OF STANDARDS-1963-A

DISTRIBUTION LIST FOR
ARL-TR-85-6
UNDER CONTRACT N00014-80-C-0490

Copy No.

	Office of Naval Research
	Department of the Navy
	Arlington, VA 22217
1	Attn: Chief of Naval Research
2	F. E. Saalfield (Code 400)
3	R. Ryan (Code 400BL)
4	E. J. Wegman (Code 411)
5	G. Hamilton (Code 420)
6	D. L. Bradley (Code 425)
7	R. F. Obrochta (Code 425AR)
8	A. Diness (Code 430)

	Commanding Officer
	Office of Naval Research
	495 Summer Street
	Boston, MA 02210
9	Attn: R. L. Sternberg

	Commanding Officer
	Naval Research Laboratory
	Washington, DC 20375
10 - 11	Attn: Code 2627

	Commanding Officer
	Naval Ocean Systems Center
	San Diego, CA 92152
12	Attn: E. Cooper

	Commanding Officer
	Newport Laboratory
	Naval Underwater Systems Center
	Newport, RI 02840
13	Attn: W. A. Von Winkle

	Commanding Officer
	Naval Air Development Center
	Warminster, PA 18974
14	Attn: H. Beyer

	Commanding Officer
	Naval Coastal Systems Center
	Panama City, FL 32401
15	Attn: J. Wynn

PREVIOUS PAGE
IS BLANK

Distribution List for ARL-TR-85-6 under Contract N00014-80-C-0490
(cont'd)

Copy No.

	Commander
	David W. Taylor Naval Ship Research and
	Development Center
	Bethesda, MD 20084
16	Attn: D. Jewell

Commander
Naval Surface Weapons Center
White Oak Laboratory
Silver Spring, MD   20910
17   Attn: P. Wessel

Commanding Officer
Naval Ocean Research and Development Activity
NSTL Station, MS   39529
18   Attn: J. Andrews

19 - 20   Commanding Officer
Defense Technical Information Center
Cameron Station, Building 5
5010 Duke Street
Alexandria, VA   22314

Director
Applied Physics Laboratory
The University of Washington
1013 N. E. 40th Street
Seattle, WA   98105
21   Attn: S. Murphy

22   Director
Applied Research Laboratory
The Pennsylvania State University
P. O. Box 30
State College, PA   16801

23   Ricky S. Bailey, ARL:UT

24   Garland R. Barnard, ARL:UT

25   H. Boehme, ARL:UT

26   C. Robert Culbertson, ARL:UT

27   Glen E. Ellis, ARL:UT

28   Loyd Hampton, ARL:UT

Distribution List for ARL-TR-85-6 under Contract N00014-80-C-0490
(cont'd)

Copy No.

29	John M. Huckabay, ARL:UT
30	Reuben H. Wallace, ARL:UT
31	Library, ARL:UT
32 - 41	Reserve, ARL:UT

END

FILMED

10-85

DTIC